[American Journal of Science, Vol. 303, October, 2003, P. 667–707]

American Journal of Science

OCTOBER 2003

PERTURBATION OF THE CARBON CYCLE AT THE MIDDLE/LATE JURASSIC TRANSITION: GEOLOGICAL AND GEOCHEMICAL EVIDENCE

GILLES DROMART*, JEAN-PIERRE GARCIA**, FABRICE GAUMET*,***, STEPHANIE PICARD*,****, MATHIEU ROUSSEAU*, FRANCOIS ATROPS*, CHRISTOPHE LECUYER* and SIMON M. F. SHEPPARD****

ABSTRACT. **A compilation of new and published stratigraphic, paleontological and geochemical data is used to detect the reciprocal influences of carbon cycling and global environmental changes in the Jurassic. A major perturbation of the surface carbon cycling accompanied by pronounced climate and sea level fluctuations (waxing and waning of continental ice?) affected Earth history around the Middle/Late Jurassic transition (MLJT). We establish the respective timing of changes of carbonate and organic matter sedimentation, and global fluctuations of sea surface temperatures (paleobiogeography and O-isotope paleothermometry) and sea level (sequence stratigraphy), so that causative mechanisms and feedback effects can be considered. It is apparent that the global sea level rise and warming initiated in the Late Bathonian led to a constriction of carbonate platforms to low latitudes and enhanced marine organic deposition. Sea level and temperature optima were achieved several million-years later during the Middle Callovian. A detailed record of sea surface temperatures in the Northern Hemisphere based on migration of marine fauna and isotopic thermometry indicates that a drastic climatic decline set in during the early Late Callovian, just post-dating the increased capture of organic matter by marine sediments. This decline in temperature is interpreted in terms of an inverse greenhouse effect, triggered by drawdown of CO_2 consequent upon excess carbon burial. The magnitude of refrigeration and its coincidence in time with an abrupt global-scale fall of sea level are both suggestive of continental ice formation at this time. Carbonate sedimentation was jeopardized at the MLJT as a result of both global cooling and presumed P_{CO_2} lowering, and resumed abruptly during the Middle Oxfordian by spreading again over mid-latitude zones. Salient conclusions are that (1) the pattern of excess carbon burial, coincident with elevated temperature but followed by climatic deterioration supports the general hypothesis that a major control on Mesozoic climate was the abundance of atmospheric CO_2; (2) significant masses of continental ice may have formed during this part of the Jurassic and correlatively, high CO_2 levels were certainly not sustained throughout this period; (3) the global carbonate sedimentation budget correlated with the surface temperature and sea level, but the latitudinal spreading of type-tropical carbonates was not simply related to the thermal status of seawaters; (4) on a global scale, the C_{org} and C_{inorg} burial rates were coupled, apparently through the correlation existing between the CO_2 level and surface temperature.**

*UMR CNRS 5125, Université de Lyon 1, Campus La Doua, 2 Rue Dubois, 69622 Villeurbanne Cedex, France ; Gilles.Dromart@ens-lyon.fr

**UMR CNRS 5561, BioGéosciences, Université de Bourgogne, 6 boulevard Gabriel, 21000 Dijon, France ; jpgarcia@u-bourgogne.fr

***Institut Français du Pétrole, 1-4 avenue du Bois-Préau, 92852 Rueil-Malmaison Cedex, France

****UMR CNRS 5570, Ecole normale supérieure de Lyon, 46 allée d'Italie, 69364 Lyon Cedex 07, France

INTRODUCTION

Mesozoic times are currently presumed to represent a typical greenhouse period of Earth history, marked by a sustained, warm and equable climate dictated by high atmospheric CO_2 levels (Hallam, 1985; Ekart and others, 1999; Berner and Kothavala, 2001; Retallack, 2001; Ghosh and others, 2001). However, sporadic climatic deterioration has also been suggested for this period (Arthur and others, 1988; Jenkyns and others, 1994; Price, 1999). The Mesozoic rock record is punctuated by a series of worldwide, stratigraphic anomalies associating C-isotope excursions, black shale formation, and episodes of carbonate platform drowning (Jenkyns, 1985; Weissert and others, 1998). Here we describe such a perturbation to the carbon cycle that occurred around the Middle/Late Jurassic transition (MLJT), namely the Callovian/Oxfordian boundary, for which it has been possible to reconstruct the respective timing of large-scale changes of carbonate and organic matter sedimentation, and global fluctuations of temperature and sea level.

The present study is based on both the acquisition and compilation of various, age-controlled data including: (1) conventional stratigraphic components [lithology, depositional environment, and age (Upper Middle and lower Upper Jurassic stratigraphic subdivisions are listed in appendix A)] gleaned from sections scattered throughout the world that straddle the MLJT; (2) the distribution and rate of carbonate accumulations; (3) organic matter content of sediments; (4) seawater paleotemperature values inferred from oxygen isotope data of biogenic phosphates and carbonates; and (5) paleogeographic distribution of marine macrofauna and continental flora. This study tests what is the necessary time resolution of geological and geochemical data to disclose genuine reciprocal interactions between variations in the carbon cycle and global environment.

CARBON PARTITIONING IN SEDIMENTS

Regional Rate and Global Distribution of Carbonate Deposition

Both sub-tropical (western Europe, Paris Basin and East-France) and inter-tropical (Middle East, Arabian Basin) Jurassic carbonate platforms have been investigated to estimate burial rates of sedimentary calcium carbonate, that is burial rates of inorganic carbon (fig. 1, appendix B). The calculation of carbonate accumulation rates is based on both the restoration of depositional volumes, by correlating stratigraphic sequences, and the estimation of carbonate concentrations from core and well-log data. A two-dimensional carbonate thickness is obtained by interpolating values among wells distributed along a stratigraphic transect (Dromart and others, 1996). A three-dimensional carbonate mass is calculated by dividing the total volume of carbonate rocks by the total surface over which wells are distributed (Dromart and others, 2002). The rates of accumulation were derived from the estimation of chronostratigraphic durations and the calibration of biostratigraphic data to the absolute time scale. In addition to the regional descriptions and calculations, plotting of worldwide deposits has been performed for successive periods around the MLJT (fig. 2), on the basis of our own observations of sections and wells in western Europe (Anglo-Paris Basin), Central Atlantic (offshore Nova Scotia), northern Africa (Algeria) and the Middle East (Oman), and data from the literature.

Middle Jurassic shallow water carbonates of the Paris Basin consist of oolitic, bioclastic deposits that built out homoclinal, low-angle ramps. The typical (sub)tropical carbonate platform that developed throughout the Bathonian over most of this basin retreated to isolated islands and marginal plateaus during the Early Callovian, prior to total drowning during the Middle Callovian, *jason* Zone (Gaumet and others, 1996; Garcia and Dromart, 1997). The deterioration of carbonate sedimentation in shallow environments materially consists of a switch from massive bioclastic and oolitic

limestones to submarine omission surfaces (lack of deposits), condensed sections rich in macrofossils (ammonites and brachiopods), and terrigenous deposits. The calculation of 3-D depositional rates has revealed that the change of carbonate sediment budgets associated with the drowning of the carbonate platform corresponds to a reduction of the net carbonate accumulation by a factor of five (fig. 1).

Globally, the Bathonian tropical-type carbonates spread symmetrically to 40° latitude (fig. 2), down to Tanzania in the Southern Hemisphere (Tanzanian Petroleum Development Corporation, 1989) and up to England (Oxfordshire; Sellwood and McKerrow, 1974; Wyatt, 1996) and Canada (southwestern Saskatchewan; Christopher, 1964) in the Northern Hemisphere. Similarly to what has been described for the Paris Basin, a drowning of Bathonian oolitic carbonate shelves has been reported from various subtropical regions of both hemispheres, for example Scotian Shelf (*Scatarie Member*, Eliuk, 1978, 1981), Somalia (*Goloda Member*, Angelucci and others, 1983), and Madagascar (*Le Bemaraha Supérieur*, Besairie, 1972). Subsequently, Middle Callovian carbonate platforms shrank considerably to low latitudes, leaving a disrupted rim in the western Tethys (fig. 2). However, regional stratigraphic documentation and mapping reveal that these Middle Callovian reefal carbonate platforms are fairly thick and exhibit a widespread coastal encroachment onto the northeastern African basement (table 1). A comparative calculation of carbonate accumulation rates from stratigraphic cross-sections of western Europe (East France) and the Arabian Peninsula (Saudi Arabia to U.A.E.) platforms reveals that similar carbonate accumulation rates for the Bathonian became strongly contrasted for the Lower-Middle Callovian (fig. 1). This comparison suggests that the carbonate sedimentation decline recorded over subtropical areas was somewhat compensated for by the coeval enhanced carbonate deposition over intertropical areas, and that the global carbonate sedimentation budget was barely altered.

The Upper Callovian and Lower Oxfordian of the Paris Basin are a succession of dark gray calcareous and silty mudstones with occasional concretionary limestone horizons and shell beds. The Callovian-Oxfordian boundary beds in the subsurface are characterized by the occurrence of iron ooids. The Uppermost Callovian of the western and northeastern margins of the basin consists of deltaic, pluri-metric thick sand deposits. Values of carbonate depositional rates are fairly low for both the Upper Callovian and the Lower Oxfordian of France (fig. 1). On a global-scale, epeiric seas became almost free of carbonate-rich sediments around the MLJT with the exception of Upper Callovian shallow-water limestones of the Middle East (Hirsch and others, 1998), and Lower Oxfordian fine-grained limestones of southern Poland (Kalna, ms, 1994), and northern Iran (Fantini Sestini, 1968) (fig. 2). Carbonate accumulation was weak over both low and middle latitude platforms (fig. 1). The data-control on oceanic sedimentation is limited because little Jurassic crust is left in modern oceans. However, the few available sites suggest that carbonate pelagic sedimentation had not invaded the oceanic realm at the end of the Middle Jurassic. Drill cores of DSDP Site 534A in the Central Atlantic contain Upper Callovian claystone whose carbonate content does not exceed 5 percent (Ogg and others, 1983). ODP Site 801 in the Old Pacific displays Callovian carbonate-free radiolarites capped by a stratigraphic hiatus involving the Early Oxfordian (Lancelot and Larson, 1990). In addition, oceanic sections now accreted to continents in the northeastern Pacific (western Canada), western Alps (Italy), and southeastern Tethys (Oman) show condensed radiolarites at the Callovian/Oxfordian transition (fig. 2).

In eastern France, carbonate sedimentation resumed during the Middle Oxfordian (Dromart, 1989). Carbonate deposits were then dominated by mud over subordinate oolitic sands plus microbial, sponge and coral buildups. A volume-based calculation of depositional rates over this area, spanning inner to outer shelf environments,

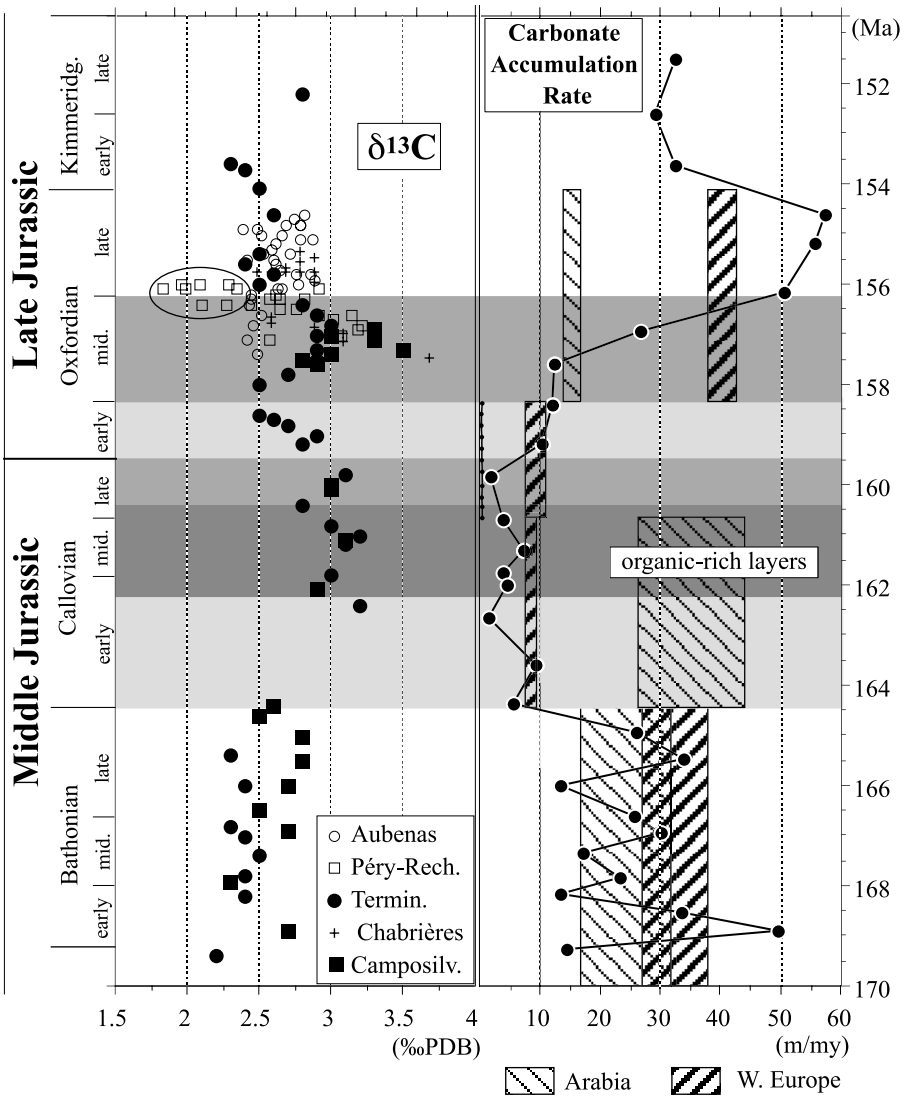

Fig. 1. Variation across the MLJT of the accumulation rates of subtropical, shallow marine carbonates in western Europe, tropical carbonate in Arabian peninsula, organic-rich deposits, and $\delta^{13}C_{carb}$ record. The solid line derives from a volume-based calculation of carbonate accumulation rates over the Paris Basin (Middle Jurassic) and Subalpine Basin (Late Jurassic) (appendix B). Hatched areas represent spans of values (minima to maxima) obtained from stratigraphic cross-sections in Arabian Peninsula and in East France (appendix B {table B2}). The Callovian organic-rich layers (O.R.L.) correspond to the stratigraphic development of the *Peterborough Mb* in England (Kenig and others, 1994), and include Middle Callovian organic-rich deposition of DSDP site 534A (appendix C {table C1}). The vertical extent of the Middle Oxfordian O.R.L. is poorly controlled. Isotope data have been repositioned against the Jurassic standard ammonite zonation (appendix A {table A1}). Bulk $\delta^{13}C_{carb}$ values come from this study (Aubenas and Péry-Reuchenette sections, appendix D {table D1}), Jenkyns (1996) (Chabrières and Camposilvano sections, appendix D {table D2}), and Bartolini and others (1991) (Terminilletto section, appendix D {table D2}). Encircled sediments from Péry-Reuchenette were deposited in waters suspected of lower salinity.

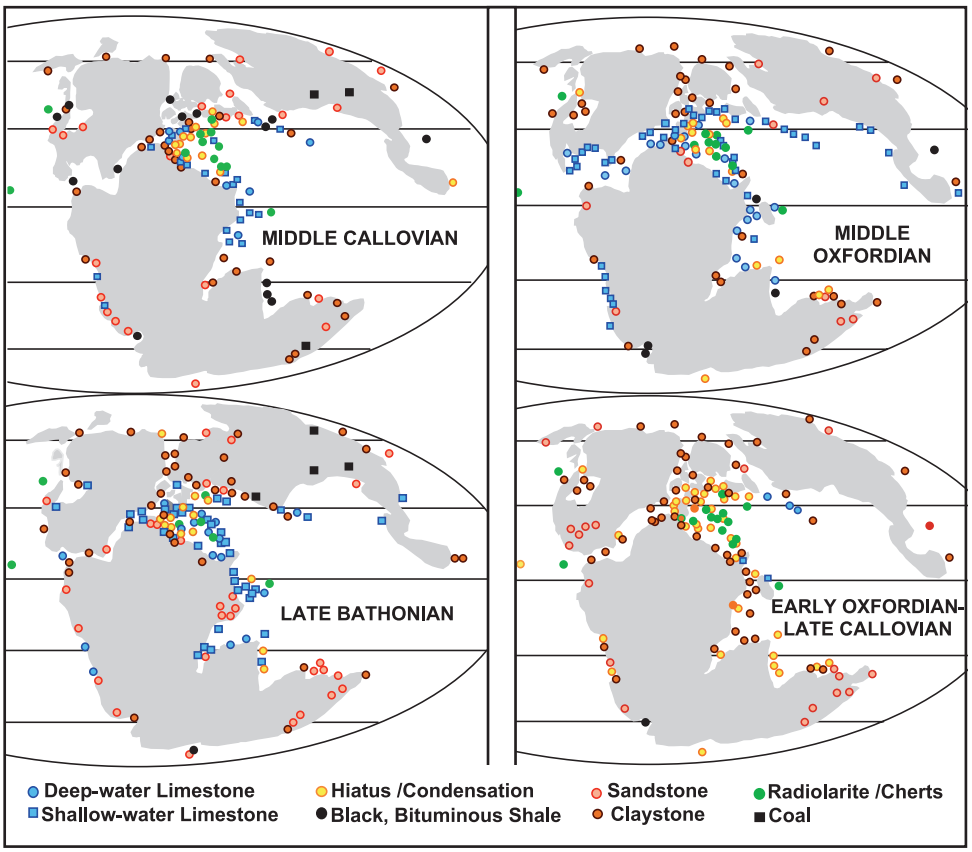

Fig. 2. Global compilation of dominant sediments at sub-stage level for the late Middle to early Late Jurassic. Land contours modified after Smith and others (1994). The maps provide a representation of the gross changes in the distribution of shallow and deep-water carbonate sedimentation through the Middle/Late Jurassic transition. They do not furnish information relative to the sediment composition and thickness and do not distinguish well and poorly biostratigraphically-identified intervals, but the sources of information are set out in a separate file available on request.

shows that carbonate accumulation rates increased four fold between the Lower and Middle Oxfordian (fig. 1). Globally, the Middle Oxfordian (sub)tropical carbonate belt re-spread to 40° latitude (fig. 2), and substantial carbonate deposition newly settled in areas such as the Gulf of Mexico (*Smackover Formation*; Imlay and Herman, 1984), and western South America (*La Manga Formation*; Legarreta, 1991).

In summary, the global carbonate sedimentation pattern changed significantly around the Middle/Late Jurassic Transition. After a widespread development of carbonate ramps throughout the Bathonian, a clear decline of carbonate accumulation affected subtropical shelves of both hemispheres while carbonate platforms widely encroached intertropical, low-relief continental basements. Subsequently, a genuine and general dearth of marine carbonate sediments marked both the uppermost Callovian and the Lower Oxfordian. Carbonate deposition then recovered significantly during the Middle Oxfordian.

Organic-rich Deposits

The organic-carbon content of a Middle Jurassic section in the Central Atlantic has been investigated. Samples from subunit 7 of the *Unnamed Formation* of DSDP Site

TABLE 1

Distribution of transgressive Callovian tropical carbonate platforms across northern Africa

Province	Location	Latitude	Longitude	Lithostratigraphy	Thickness (m)	Skeletal components	Age	Paleo-latitude [1]	Basement	Reference
W. Morocco	Aguadir Basin	30°26'N	9°20' W	Ouanamane	100	stromatoporoids, foraminifers	Early-Middle Callovian	24°N	M. Jurassic marginal marine hydrid rocks	Peybernes and others, 1987
N. Sahara	Ghardaia Hr 8	32°30'N	3°05'E		100	corals, foraminifers	M. Callovian	22°N	M. Jurassic marginal marine hydrid rocks	Busson, 1972
N. Sahara	Erg oriental Gef 1	31°42'N	7°58'E		160	corals, foraminifers	M. Callovian	20°N	M. Jurassic marginal marine hydrid rocks	Busson, 1972
Dahar	Tataouine	32°55'N	10°27'	Foum Tataouine	95	coral bioherms	M. Callovian	20°N	M. Jurassic marginal marine hydrid rocks	Ben Ismail and others, 1989
Quattara	Betty 1 well	29°40'N	27°26'E		130	foraminifers	Middle-Late Callovian	10°N	M. Jurassic fluvial sandstones	Said, 1962
Sinai	Jebel Maghara	30°42'N	33°23'E	Zohar	100	corals, oncholites	Middle Callovian	8°N	M. Jurassic marginal marine hydrid rocks	Hirsch, 1980
Negev	Jebel Kurnub	30°58'N	34°58'E	Zohar	100	stromatoporoids, corals	M. Callovian (coronatum Z)	8°N	M. Jurassic marginal marine hydrid rocks	Hirsch and others, 1998
C. Saudi Arabia	Darb al Hijaz	24°15'N	46° 19'E	Tuwaiq Lst.	215	stromatoporoids, corals	M. Callovian (coronatum Z)	2°S	M. Jurassic shallow marine limestones	Powers and others, 1966
N. Yemen	Sana'a	15°45'N	43°45'E	Al-Khotally	45	stromatoporoids, corals	Middle-Late Callovian	8°S	Unconformity: Precambrian Basement	Al-Thour, 1997
Eritrea	Mahur	14°26'N	40°50'E	Antalo Limestone	80	hydrozoans, foraminifers	Middle-Late Callovian	9°N	M. Jurassic fluvial sandstones	Sagri and others, 1998
Yemen	Amal-4 well	14°58'N	46°32'E	Shuqra	350		M. Callovian (coronatum Z)	11°S	Unconformity: Precambrian Basement	Sharland and others, 2002
Yemen	Jabal Madbi	14°12'N	48°01'E	Shuqra	47		Middle-Late Callovian	12°S	M. Jurassic fluvial sandstones	Beydoun, 1966

(1) estimated from Smith and others, 1994

534A (Ogg and others, 1983) have been analyzed for organic matter (OM) using the Rock-Eval pyrolysis method (Rock-Eval II with a carbon module; Espitalié and others, 1985). Age assignments were derived from the dinoflagellate assemblages (Habid and Drugg, 1983). The Middle Callovian subunit 7c is 8 meters thick, and is composed of a laminated, greenish black to olive black claystone. The total organic carbon (TOC) values range from 1.1 to 3.3 percent by weight (appendix C). The OM is terrestrial with marine admixtures (dinoflagellates and amorphous debris) when the TOC is high (Summerhayes and Masran, 1983). Consistently, hydrogen index (HI) values rise (type III to type II kerogen) as the organic content increases (appendix C). Higher up, the OM content significantly decreases across the Middle/Upper Callovian transition, and is very low in the variegated Oxfordian sediments.

Other reference sections for the Callovian organic-rich deposits are the *Peterborough Member* (Pt Mb) of the *Oxford Clay Formation* in England (Kenig and others, 1994), and the *Tuwaiq Mountain Formation* in Saudi Arabia (Carrigan and others, 1995). The Pt Mb, 17 meters thick at Peterborough, has been allocated to the uppermost Lower Callovian - lowermost Upper Callovian on the basis of ammonite biostratigraphy. It typically comprises dark greenish gray, shelly mudstone, with minor cyclicity involving the alternation of dark gray, very fissile units and firmer, blocky, slightly paler mudstones (Hudson and Martill, 1994). The TOC content is up to 16.6 percent and mostly above 3 percent by weight. Amorphous OM, made up of marine algal matter of phytoplanktonic origin, dominates (85 up to 95%) organic-rich shales. The organic richness of the Pt Mb contrasts with the depletion of OM in the underlying and overlying units, both lower than 1.5 percent TOC. *The Stewartby Member* (Upper Callovian) contains much less amorphous OM, and the structured OM is composed of very small-sized and angular coaly debris reflecting a long residence time in an oxygen–rich water (Belin and Kenig, 1994). Above, the *Weymouth Member* (Lower Oxfordian) is also depleted in organic carbon with all concentrations under 1 percent. In the southern Arabian Basin, the organic-rich interval of the *Tuwaiq Formation* is up to 150 meters thick. The organic matter is dominated by lamalginite with high hydrogen indices. The lamalginite consists of leiosheres, which form fine, but very distinctive laminae in peloidal carbonate packstone. The TOC content averages 3 weight percent with values up to 13 weight percent. The *Tuwaiq Formation* has been assigned to the Middle and Upper Callovian in Arabia on the basis of ammonite biostratigraphy (Enay and others, 1987; Hirsch and others, 1998).

Coincidentally with the modification of inorganic carbon storage in the carbonate surface reservoir, the organic sedimentation pattern evolved through the Middle/Late Jurassic Transition. Continental to marginal marine Bathonian coal accumulations gave way to very scattered Middle Callovian marine organic-rich sequences (table 2). Enrichment in OM of Callovian can be documented from many low- and mid-latitude localities all around the world (table 2). Deposition of organic-rich layers occurred in both epeiric seas (western Europe and Arabian Peninsula) and narrow deep troughs (Atlantic seaway and Mediterranean area) throughout the Middle Callovian - early Late Callovian interval. In contrast, Lower Oxfordian shaley sediments are fairly poor in OM and contain a relatively large amount of land-sourced, oxidized organic debris. Again, the Middle Oxfordian is commonly represented by fissile, asphaltic, organic-rich sediments: *Hanifa Formation* in the Arabian Peninsula (Droste, 1990) and Basal *Smackover Formation* in the U.S. Gulf Coast (Heydari and Wade, 2002).

Carbon Isotope Record

Stable-isotopic analyses have been carried out on bulk carbonate samples coming from two Callovian-Oxfordian sections located in northeastern Switzerland (Pery-Reuchenette section; Gygi and others, 1998) and southeastern France (Aubenas-Chanabier section; Dromart, 1989) [appendix D (table D1)]. Both sections corre-

TABLE 2

Distribution of organic-rich deposits for the Bathonian (coals) and Callovian (bituminous marine shales)

	Province	Location	Lithostratigraphy	Lithology (TOC max)	Age	Paleo-latitude [1]	Reference
Callovian	S. England	Peterborough	Peterborough Mb	fissile, dark gray mudstone (16.6%)	late E. to early L. Callovian *(endatum to phenium SZ)*	38°N	Kenig and others, 1994
	C. Atlantic	ODP 534 A	Unnamed Fm, 7c-7e	laminated claystone (3.3 %)	M. to L. Callovian	15°N	Sheridan & Gradstein, 1983
	W. Scotland	Skye Island	Dunans Shales Mb	laminated bituminous shales (10.4%)	M. Callovian	44°N	Morton, 1987
	E. Paris Basin	HTM 102 well	Argiles de la Woëvre Fm	green-colored claystone (1%)	M. Callovian (*jason* Z)	35°N	Landais & Elie, 1999
	W. Greece	Ionan Zone	Epirus Radiolarites	radiolarites (8.6%)	Callovian	20°N	Danelian & Baudin, 1990
	Kurdistan	Urmia lake		bituminous shales	M. Callovian *(anceps* Z)	32°N	Arkell, 1956
	Saudi Arabia	Khurais	Tuwaiq Mountain Fm	laminated mud/packstone (13%)	late M. to early L. Callovian (*coronatum* to *athleta* Z)	5°S	Carrigan and others, 1995
	Philippines	Mindoro	Mansalay Formation	black shales, carbonaceous sands	E. - M. Callovian	23°N	Andal and others, 1968
	C. Oregon	Izee area		organic-rich mudstone	M - L. Callovian	36°N	Poulton, 1992
	S. Mexico	Guerrero, Cualac		bituminous shales	Callovian	10°N	Arkell, 1956
	E. Falkland	DSDP 511		laminated shales	M. Callovian *(coronatum* Z)	50°S	Ludwig & Krasheninnikov, 1983
Bathonian	North Sea	East Shetland Basin	Tarbert Formation	coal seams	Bathonian	50°N	McLeod and others, 2002
		South Viking Graben	Sleipner/Hugin Fm	coal seams (lacustrine)	Bathonian-Callovian	47°N	Isaksen and others, 2001
		Danish Central Graben	Bryne Formation	coal seams (coastal plain)	Bathonian	43°N	Petersen and others, 1996
		East Scotland	Brora Coal Formation	coal seams (coastal plain)	L. Bathonian	45°N	Underhill & Partington, 1993
	S. France	Grands Causses	Calcaires à Stipites	lignite (marginal marine)	M. to L. Bathonian	31°N	Charcosset, ms, 1998
		Quercy	Formation de Cajarc	lignite (marginal marine)	M. Bathonian	31°N	Delfaud, ms, 1969
	Great Caucasus	Pskhu, Abkhasia	Betaga Suite	coal lenses	E. Bathonian	37°N	Topochishvili and others, 1998
		Tkibuli, Georgia		coal seams	Bathonian	36°N	Barale and others, 1991
		Tsudakharskaya, Daghestan		coal seams	Bathonian	38°N	Bergerat and others, 1998
		Karabulak, Stavropol		coal seams	Bathonian	38°N	Bergerat and others, 1998
	N.W. China	Turpan Basin	Jurassic Coal Measures	coal seams (fluvial)	Middle Jurassic	50°N	Hendryx and others, 1995
		S. Junggar Basin	Jurassic Coal Measures	coal seams (fluvial)	Middle Jurassic	50°N	Hendryx and others, 1995
	E. Australia	New South Wales	Walloon Coal Measures	coal seams (fluvial, lacustrine)	Middle Jurassic	70°S	Othman & Ward, 2002
		Maryborough	Tiaro Coal Measures		Bathonian	72°S	Bradshaw & Chalinor, 1992
	Levant	Jebel Magarah, Sinai	Safa Formation	coal seams	E. Bathonian	7°N	Mostafa & Younes, 2001
		N.Negev, Queren 1 well	Sherif Formation	coal seams	E. Bathonian	7°N	Goldberg & Friedman, 1974
	E. Sahara	W. Mursuq Basin	Taouratine Formation	coal	Middle Jurassic	16°N	Jakovljevic and others, 1991
		Tinrhert, Es 101 well		coal	Bathonian	17°N	Busson, 1972
		Hassi R'Mel 3 well		coal	Bathonian	20°N	Busson, 1972

(1) estimated from Smith and others, 1994

spond to outer shelf depositional environments of the northeastern Tethyan margin. Samples are composed of fine-grained, platform-derived carbonate sediments. $\delta^{13}C_{PDB}$ values range from 1.6 to 3.2 permil. The lack of covariance of $\delta^{13}C_{PDB}$ and $\delta^{18}O_{PDB}$ suggests that the C-isotopic composition of the samples has not been altered significantly by burial diagenesis [appendix D (fig. D1)]. In addition to this data set, we have integrated data from Bartolini and others (1996) and Jenkyns (1996) [appendix D (table D2)] to produce a continuous carbon isotope curve for the Tethyan pelagic limestones of the Lower Callovian - Upper Oxfordian interval (fig. 1). There are two small positive $\delta^{13}C_{carb}$ excursions, with values exceeding 3 permil, in the Middle-Upper Callovian and Middle Oxfordian. Consistently, relatively high values (around 3‰) have been recorded from aragonite macrofossils (nuculacean bivalves and ammonites) in the *Peterborough Member* of the *Oxford Clay* (Anderson and others, 1994). These values probably cannot be directly compared with the bulk carbonate data without subtracting 0.8 permil, an average bioaragonite – biocalcite fractionation factor.

Middle Callovian and Middle Oxfordian $\delta^{13}C_{carb}$ optima are typically coincident in time with the episodes of organic-rich sedimentation (fig. 1). To date, the very limited amplitude of these positive inflexions is interpreted to reflect the concomitant sustainability of carbonate burial rates. The $\delta^{13}C$ signal at the MLJT (Upper Callovian - Lower Oxfordian interval) has apparently been buffered by the combined decline of both organic and carbonate sedimentation.

The C-isotope data gleaned from various Callovian-Oxfordian sections of the Tethys are currently consistent with the modification of the carbon partitioning between the C_{org} and C_{carb} sinks as suggested by the geological observations. However, the amplitude and exact timing of the positive $\delta^{13}C_{carb}$ excursions have to be further substantiated so that C-isotope data can be used as a tool to characterize the carbon cycle perturbation. In particular, current $\delta^{13}C_{carb}$ data from the Middle-Upper Callovian and Lower Oxfordian are definitely too scarce and poorly dated.

GLOBAL ENVIRONMENTAL CHANGES

Sea Level Changes

Restoration of sea level fluctuations is derived from the analysis of facies sequence data of stratigraphic descriptions from different sites of the world. From the Bathonian to the Oxfordian there is a secular trend toward a rise in sea level that is punctuated by widespread apparently synchronous deepening and shallowing events, which represent global sea level fluctuations (table 3). Evidence for the positive long-term trend comes from plotting the areas covered by sea in successive Jurassic stages (Hallam, 1978, 1988; Smith and others, 1994).

At a higher degree of resolution, the Middle-Upper Bathonian displays a typical coastal encroachment of marginal marine deposits upon continental areas, together with an abrupt onset at distinct moments of genuine marine conditions in many places of the world. In particular, a latest Bathonian marine flooding event is recorded all across northern Europe, and has a definite global echo (table 3). The worldwide Early to Middle Callovian transgressive event is also a pronounced feature of Jurassic history (Hallam, 2001), and there is a definite trend of positive eustasy that developed from the Late Bathonian to the Middle Callovian. Locally, regressive events punctuated this evolution, at the end of the Bathonian (Li and Grant-Mackie, 1993) and during the earliest Callovian (Gaumet and others, 1996). The sporadic record of these events probably owes its origin to the limited magnitude of related sea level falls.

In contrast, the Late Callovian regressive event is conspicuous in many places over the world (table 3), marked by various sedimentological features: 1) calcareous low-density turbidites off Blake Plateau, West Central Atlantic (Ogg and others, 1983); 2) calcareous shales bearing quartz sands and ferruginous oolites at the margins of the

TABLE 3

Worldwide transgressive/regressive events in early Late and late Middle Jurassic times

Events	Europe	World
Middle Oxfordian Transgression	W-Scotland - Skye Island E-Scotland - Ross Field North Sea - Witch Ground Gb E-Russia - Moscow Area NW-France SE-France - Alpes maritimes NE-Iberia Portugal - Algarve-Lusitania Georgia	S- & E-Mexico U.S. Gulf Coast W-Siberian Basin
Late E. Oxfordian Transgression	SE-France - Causses NE-Iberia	W-Israel - Coastal Plain Alaska Peninsula W-Canada - Alberta Trough W- Argentina - Neuquen Province Philippines, S-Mindoro
Late Callovian Regression	E-Greenland E-Scotland - Moray Firth W-Norway - Horda PF NE-France -Ardennes NW-France - Perche S-France - Quercy NE-Iberia Portugal - Algarve-Lusitania	NW-Algeria NE-Sahara W-Israel - Coastal Plain NE- Saudi Arabia N-Oman E-Japan - Hida Mountains E-Siberia - Olomon Platform Alaska Peninsula W-Canada - Alberta Tr. - Williston B. W-Atlantic - Blake Plateau W-Argentina - Neuquen Province NW-Australia Philippines, S-Mindoro NE-Madagascar
Middle Callovian Transgression	SE-France - Causses N-France - Boulonnais S-Baltic Georgia - Bzibi River C-Portugal	N-Iran - Elbruz Mountains NE-Ethiopia C-Saudi Arabia Yemen N-Algeria - Ouarsenis NE-Sahara
Callovian Transgression	SE-France - Briançonnais SE-France - Var Georgia - Veluanta	W-Morocco - Aguadir Basin E-Canada - Scotian Shelf W-Canada - Williston Basin S-Tibet - N-Lhassa
Early Callovian Transgression	E-Greenland W-Scotland - Skye Island E-Scotland - Moray Firth Faroe-Shetlands, Shetlands E-England - Lincolnshire E-Russia - Moscow Area	Central Russia - W-Siberia Central Morocco - Middle Atlas

TABLE 3
(continued)

Events	Europe	World
Late Bathonian	E-Greenland	W-Madagascar
Transgression	E-Scotland - Moray Firth*	W-India - Kachchh Mainland
	W-Scotland - Hebrides Basin	C-Nepal - Thakkhola Area*
* Latest	E-England - Lincolnshire*	Japan - Hida Mountains*
Bathonian	N-France - Boulonnais*	NW-Canada - Porcupine River*
	C-France - Burgundy*	NE-Canada - Grand Banks
	SE-France - Causses	S-Mexico
	SE-France - Haut Var	C-Peru - Ayacucho Area
	S-France - Quercy*	? NW-New Zealand
	W-Sicily - Trapanids	W-Siberian Basin
	S-Spain - Betic Ranges	NE-Sahara
	E- Romania - Dobrogea*	
	E-Russia - Moscow Area*	
	E-Abkhasia	
Middle - Late	W-Scotland - Beatrice Field	W-Morocco - Aguadir Basin
Bathonian	N-France - Boulonnais	S-Tunisia (Medenine)
Aggradation	N-Germany - Hanovre Area	NE-Ethiopia
(Coastal onlap)	SE-France -Cévennes	N-Egypt - Suez Gulf
	S-France - Quercy	W-India - Kachchh Mainland
	W-Alps - Briançonnais/ Valais	C-Peru - Ayacucho Area
	S-Poland - Cracow Area	W-Canada - Sweetgrass Arch
	E-Romania - Dobrogea	W-USA - S-Utah
	E-Russia - Moscow Area	

Uncertainty associated with the dating is not expressed but information sources are available in a file of references. The transgressive events are reliably and finely datable because they correspond to condensed deposits rich in adequate fauna, e.g. ammonites and/or brachiopods, whereas regressive counterparts bear larger age uncertainty because associated proximal sediments have experienced subaerial exposure and erosion leaves no appropriate fossil record.

Paris Basin (Juignet and Lebert, 1986; Curial and Dromart, 1998); 3) progradational shoreface sandstones around the North-Sea (*Fensford*, Horda Platform, Jacquin and others, 1998; *Olympen*, eastern Greenland, Surlyck, 1991; *A Sand*, Moray Firth, Underhill and Partington, 1993); 4) paleokarsts in western Portugal (Azerêdo and others, 1998), Israel (Hirsch and others, 1998), and northern Oman (Lekhwair area); 5) subaerial incised valleys in South-Portugal (Rocha and Marquez, 1979) and northeastern Saudi Arabia (Powers and others, 1966). Additional supporting evidence for a sea level lowstand comes from the occurrence of siliciclastic depositional systems loosely dated as [U. Callovian - L. Oxfordian], for example high-density turbidites in northwestern Algeria (Benest and others, 1995) and alluvial fan deposits in western Argentina (Gulisano and Gutierrez-Pleimling, 1994). Regional observations in Lusitania, Portugal (Azerêdo and others, 1998), reveal a sea level fall with amplitude attaining at least several tens of meters. The compilation and comparison of biostratigraphic data indicate that the sea level lowstand must have occurred during the Late Callovian, around the *henrici/ lamberti* Subzone boundary (Dromart and others, 2003).

This argument for a eustatic sea level fall in the Late Callovian is in agreement with an initial evaluation of Jurassic eustasy by Hallam (1978, 1988). However, it contradicts the interpretation by Norris and Hallam (1995) that the Callovian-Oxfordian boundary is a highstand in eustatic sea level. Their view was derived from the analysis of western European sections for which it is tricky to restore sea level

fluctuations because there is abundant evidence of extreme condensation for the Callovian-Oxfordian deposits (stratigraphic hiatus, ammonite-rich horizons, iron ooidal limestone beds). The difficulty in analyzing correctly this type of facies is illustrated by the fact that sections in the Iberian Chain were interpreted in opposite ways by Aurell and others (1994) and Norris and Hallam (1995). This divergence of views comes from the occurrence of both shallow (iron oolites) and pelagic (biomicrites, ammonites) features in sediments. Rapid and high-amplitude sea level oscillations associated with the waning and waxing of continental ice through the MLJT could reconcile these contradictory arguments.

A transgressive regime resumed by the latest Callovian in north western Europe (northern North-Sea, Jacquin and others, 1998; Paris Basin, Curial and Dromart, 1998), Russian and western Siberian Platforms (Sahagian and others, 1996; Pinous and others, 1999), northeastern Siberia (Sey and others, 1992), northwestern United States (Poulton and others, 1992), and pulsed in the late Early Oxfordian, earliest *cordatum* Zone. After a brief regressive event at the Early/Middle Oxfordian transition (Underhill and Partington, 1993; Sahagian and others, 1996; Pinous and others, 1999), transgressive conditions generally prevailed during the Middle Oxfordian (table 3).

Seawater Temperatures

Temperatures of the upper seawater of northwestern Tethys (fig. 3) have been calculated from oxygen isotopic ($\delta^{18}O$) composition of apatite enamel from shark (*Asteracanthus, Sphenodus*) and fish (pycnodonts) teeth [appendix E (table E1)]. All analyzed Jurassic teeth come from shelfal, open marine environments of eastern France and western Switzerland (paleolatitude ranging from 30° to 36°N) with supporting evidence, using the approach of Picard and others (1998), that the fish and sharks were surface or near-surface water dwellers. Potential problems of diagenetic alteration of isotopic ratios of samples used through this study have been addressed by Lécuyer and others (2003). No diagenetic perturbation has been detected during chemical procedures. Moreover, all samples plot inside the domain of apparent oxygen isotopic equilibrium between phosphate and carbonate from the same bioapatite (Lécuyer and others, 2003). These observations strongly suggest that primary isotopic compositions have been preserved.

Calculated isotopic temperatures depend directly upon the assumed value of $\delta^{18}O_{sw}$. For an ice-free world, –1 permil is usually selected, as here. The actual value is principally a function of the mass of any continental ice reservoir and its mean $\delta^{18}O$ value, and the salinity of the seawater at the latitude of interest. By analogy with the modern oceanographic – climatic system, subtropical waters are typically enriched in $\delta^{18}O$ by 0.5 to 1.3 permil relative to the mean ocean waters (Railsbach, 1990). For this reason Lécuyer and others (2003) took a $\delta^{18}O_{sw}$ to be 0 permil for Middle to Late Jurassic subtropical waters and their calculated isotopic temperatures are about 4°C higher than those presented below.

O-isotope data indicate warm subtropical surface seawaters (~20°-27°C for a $\delta^{18}O_{sw}$ of –1‰) for the Bathonian platform of eastern France. Temperatures then apparently increased a little during the Early and Middle Callovian, coincidentally with the incursion of both Tethyan and boreal ammonite fauna into the area (Marchand and Thierry, 1997) (fig. 3). This faunal mélange is interpreted here to be the product of changing physiographic conditions. The warming of low-latitude waters was associated with a concomitant rise of sea level that presumably enabled boreal fauna to migrate over transverse barriers, for example the London-Brabant High (Garcia and others, 1996), and to mix with their southern counterparts. However, no correction has been made to the temperature calculation to take into account the potential introduction of isotopically light boreal waters because cold and dense boreal waters were likely directed down to the incipient Central Atlantic through a number of deep

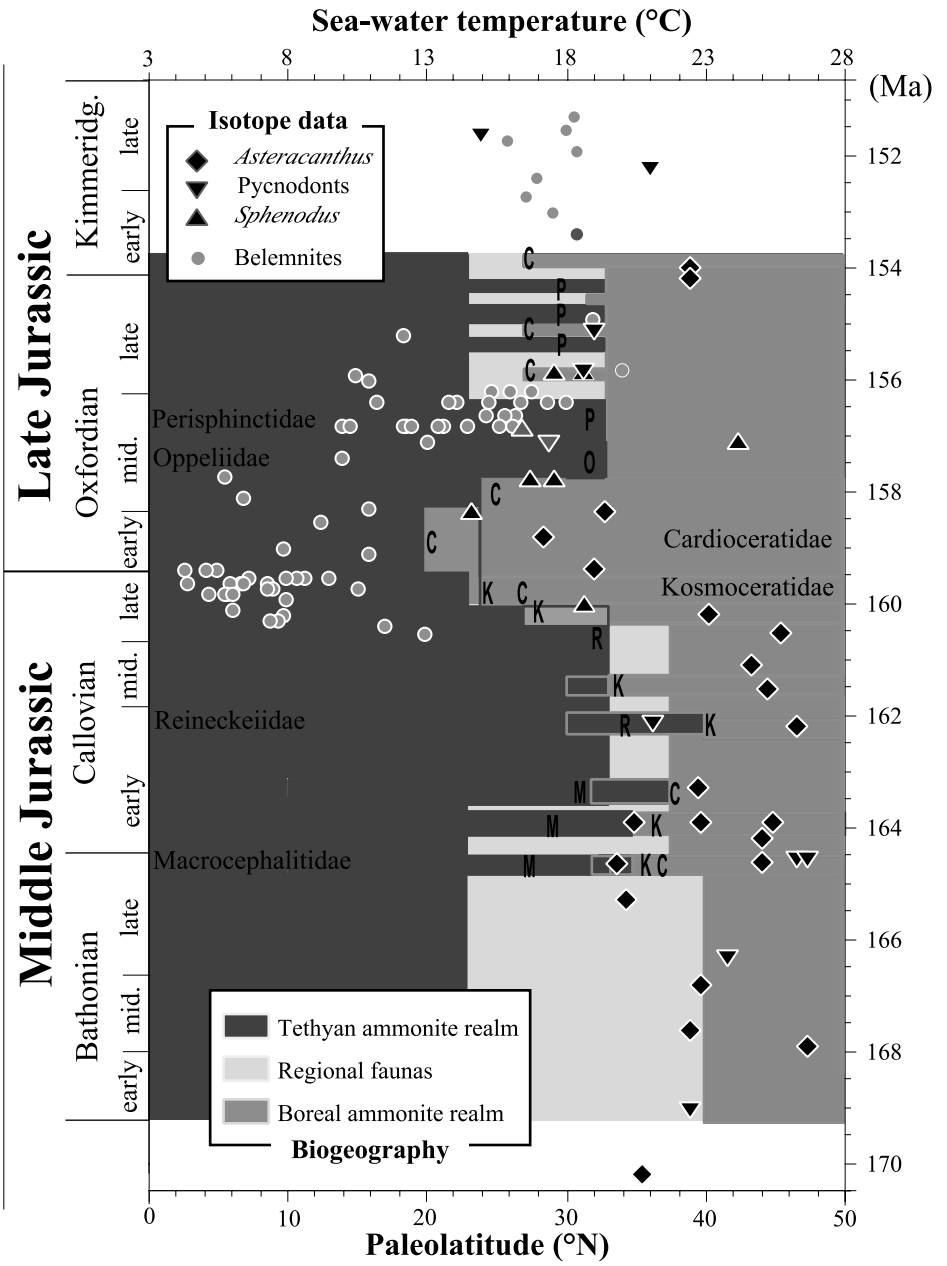

Fig. 3. Variation across the MLJT of mid to surface seawater paleotemperatures, and paleolatitudinal expansion of Tethyan and boreal ammonites, western Europe. O-isotope data used to calculate seawater temperatures are provided in appendix E.

troughs (Rockfall Trough, Celtic Sea Basin; Ziegler, 1988) and they did not flow over the studied platforms.

A pronounced decline of seawater temperatures started in the early Late Callovian (*athleta* Zone), and was marked by an apparent drop of ~6°C of eastern France surface

waters, cooling down to ~15° to 19°C (fig. 3). The belemnite $\delta^{18}O$ data from the MLJT of the United Kingdom as well as from western Russia [appendix E (table E2)] show a similar abrupt shift to heavier values, interpreted as due to climatic deterioration (Jenkyns and others, 2002). The seawater cooling implied by O-isotope paleothermometry is coincident in timing with the retreat of Tethyan ammonites from mid-latitude zones and expansion of boreal forms into low-latitude seas (fig. 3). Tethyan Reineckeidae disappeared from northern France at the end of the *athleta* Zone (Cariou, 1984). Conversely, boreal Kosmoceratidae settled in southern Europe throughout Late Callovian times, reaching southeastern France and central Portugal during *athleta* Zone (Cariou and others, 1985) then south Portugal (Algarve) during *lamberti* Zone (Da Rocha and Tintant, 1974). A subsequent wave of boreal ammonites, that are Cardioceratidae (*Quenstedtoceras*, *Cardioceras*), invaded southeastern France during the latest Callovian (*lamberti* Subzone) (Fortwengler, 1989). During the Early Oxfordian, Cardioceratidae decreased in relative abundance in southeastern France (50% down to 5-15% of the ammonite assemblage; Fortwengler and others, 1997) but extended down to northern Africa (20°N paleolatitude) in northern Algeria (Cariou and others, 1985) and Morocco (Ambroggi, 1963).

The sudden retreat of Cardioceratidae to the boreal province with reciprocal massive invasion of Tethyan forms, that are Oppeliidae (*Taramelliceras*), marked in west Europe the passage between the *vertebrale* and *antecedens* Subzones of the early Middle Oxfordian (southeastern France; Bourseau, 1977). This event coincided in time with the re-deposition of oolitic/coral carbonates in northwestern Switzerland (*Saint Ursanne Fm*; Gygi and others, 1998) and southern England (*Osmington oolite* and *Coral-rag*; Wright, 1981, 1986). The rapid onset of type-tropical carbonates along with the sharp change of ammonite hegemony suggest a much more abrupt warming in the Middle Oxfordian than do the O-isotope data of vertebrate phosphates (fig. 3).

In summary, both the isotopic and paleontological data are consistent with a drop in temperature of western Europe surface seawater during the early Late Callovian, and an increase during early Middle Oxfordian times. Confirmation of the climatic deterioration around the MLJT comes from paleofloral data such as palynomorph associations observed in the North Sea (Abbink and others, 2001), and the presence of *Xenoxylon* plants in the Upper Callovian and Lower Oxfordian of Germany and France (Philippe and Thevenard, 1996), both of which are diagnostic of the onset of chilly and humid conditions on northern Europe hinterland. The subsequent question is to determine whether this cooling event is regional or global in nature, and whether a change of 6°C for subtropical seawater is tenable or not.

Evidence of seawater cooling in Eurasia is supported by the presence of boreal ammonites that is *Quenstedtoceras*, in the Upper Callovian and Lower Oxfordian in Georgia (Topchishvili and others, 1998) and northern Iran (~30°N paleolatitude) (Seyed-Emani and others, 1995). O-isotope data on belemnites of northeastern Russia consistently indicate that seawater temperatures were lowest at the MLJT and increased from ~7° to 15°C during the Middle Oxfordian (fig. 3). The warming is also recorded by the northward 15° to 20° latitudinal shift of the subtropical forest belt of "former USSR" during the Early - Middle Oxfordian (Vakhrameev, 1981). In Central Asia (North China), the onset of hot, and semiarid to arid continental conditions, which continued throughout the Late Jurassic (Sarjeant and others, 1992; Hendryx and others, 1995; Ritts and others, 1999) appears to record this climatic change. In the northwestern Pacific, western Interior Canada, boreal faunas (60°N) spread southward during the Late Middle Jurassic (Poulton, 1984). Boreal *Quenstedtoceras* has been documented in the Upper Callovian of Montana, and a sequence of *Cardioceras* has been observed in the Lower and Middle Oxfordian down to northern Utah (~30°N paleolatitude) (Poulton and others, 1992). A weaker southward expansion of boreal

faunas is recorded on the other side of the North Pacific from 75° to 60°N (Parrish, 1992). We conclude that the whole of the northern hemisphere endured a genuine cold period that began in the early Late Callovian and apparently lasted throughout the Early Oxfordian. A Middle Oxfordian thermal recovery was more effective in the northwestern Tethys than in the Pacific realm where chilly conditions apparently lingered (Parrish, 1992).

Polar Ice: Waxing and Waning

The worldwide sea level fall and rise during Late Callovian and Middle Oxfordian, respectively, covary with decreasing and increasing temperatures of surface seawater in Europe. Such a correlation of relatively rapid eustatic sea level changes with seawater temperatures is very suggestive of waxing and waning of continental ice.

Direct evidence for high-latitude freezing conditions at the MLJT comes from the Callovian-Oxfordian sediments of Siberia that contain star-shaped carbonate concretions that are glendonite (Chumakov and Frakes, 1997). The potential formation of continental ice has immediate implications for the paleotemperature calculations (fig. 3) that used a $\delta^{18}O$ seawater of –1 permil (SMOW), the reference value for an ice-free world. If continental ice was present around the MLJT then the proposed paleoisotopic temperatures of ~15° to 19°C (fig. 3) need to be increased, and the amplitude of the thermal drop during the Late Callovian reduced. The glacial isotopic temperatures of eastern France have been calculated to be 2° to 4°C higher than the model values with $\delta^{18}O_{sw} = -1$ (fig. 3) on the basis of an estimate of the mass of continental ice involved and assuming an ice O-isotope composition of –30 permil (Dromart and others, 2003). The revised net cooling of 2° to 4°C recorded for the subtropical surface seawaters of the MLJT is very similar to estimates for Quaternary interglacial to glacial episodes (Broecker, 1995).

It has been previously inferred that the sea-level minimum was reached at the *henrici/ lamberti* Subzone transition in the latest Callovian. The implication of this is that ice cap formation and maximum decline of surface seawater temperatures should have occurred during the Late Callovian and not the Early Oxfordian, as suggested by the O-isotope paleothermometry and optimal southern extent of boreal ammonites in the northwestern Tethys (fig. 3). This conflict may only be apparent in that: 1) sampled teeth are certainly not in sufficient number to pin down precisely the thermal minimum; 2) inappropriate depositional conditions (high sedimentation rate or erosional hiati) may have precluded the finding of boreal ammonites in the Upper Callovian of southern areas. The occurrence of a widespread regressive event by the end of the Early Oxfordian suggests that glacial conditions were maintained throughout this interval of time.

In conclusion, it can be stated that in general sea level and seawater temperatures changed in concert around the MLJT, the most striking feature being the exact coincidence between the sea level fall and the cooling of seawater during the early Late Callovian, *athleta* Zone. This correlation is indicative of the development of continental ice caps. Apparently, the global sea level rise started slowly as early as latest Callovian times while seawater temperatures remained relatively low. The Jurassic Glacial Maximum is estimated to have occurred during the *lamberti* Zone of the Late Callovian, that is 159.6 Ma (Gradstein and others, 1994).

NORMAL AND INVERSE GREENHOUSE EFFECTS

For geologic time scales, the atmospheric CO_2 concentration is assumed to be regulated by inputs from volcanism and, possibly, by gas hydrate dissociation, and uptakes by the biological pump and the weathering of silicate rocks. Variations of the atmospheric CO_2 level are considered to be a major driving force of back and forth oscillations between cold and warm conditions at the Earth's surface.

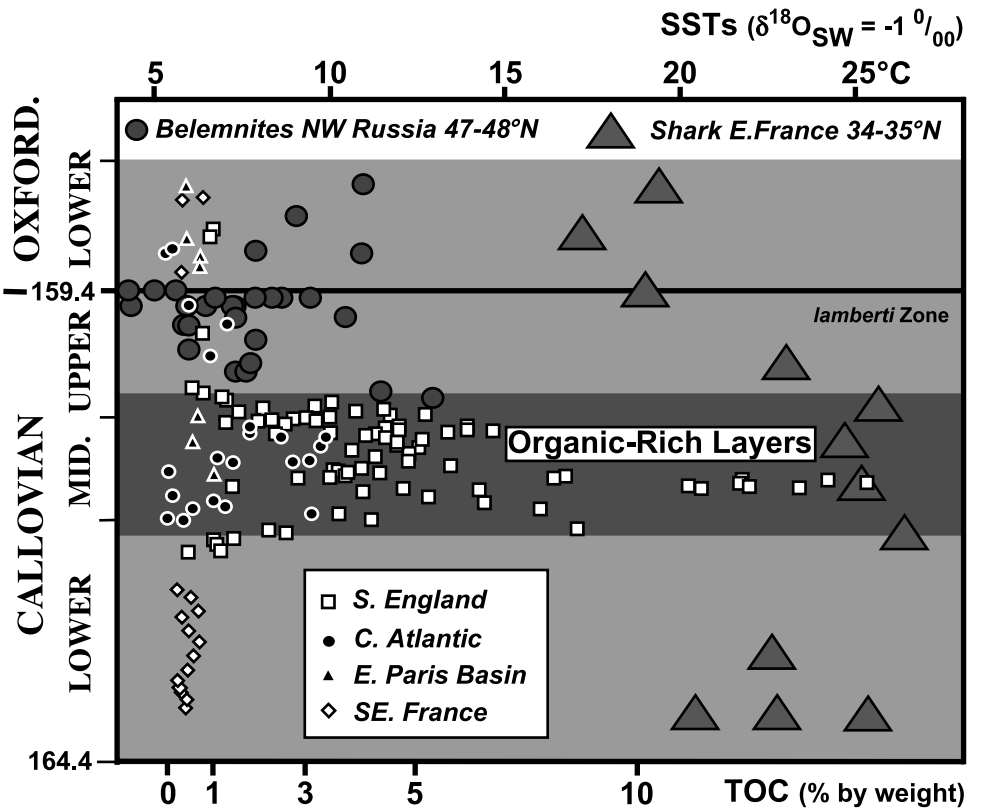

Fig. 4. Covariation of the organic matter content of Callovian-Oxfordian marine sediments of western Tethys and Surface Seawaters Temperatures (SSTs) of northeastern and western Europe. The Total Organic Content (TOC) is derived from pyrolysis analysis. This TOC database is a compilation of new data (Central Atlantic, ODP 534A, appendix C) and published values: S-England, Kenig and others, 1994; E-Paris Basin, Landais and Elie, 1999; southeastern France, Dromart and others, 1989. O-isotope data used to calculate SSTs are provided in appendix E. Only *Asteracanthus* (shark) samples have been presented for eastern France.

Normal Effect

Middle Callovian thermal optimum.—The deposition of the Middle Callovian organic-rich shales is correlated with a thermal optimum of seawater and a sea level highstand (figs. 4 and 5). A similar coincidence has been suggested for the Cenomanian-Turonian (Arthur and others, 1988; Jenkyns and others, 1994) and the Toarcian (Jenkyns and Clayton, 1997) anoxic events. Currently, we cannot assess the respective contribution to the organic enrichment of productivity promoted by high [$CO_{2(atm)}$] and enhanced preservation of organic matter due to lower solubility of oxygen by increased seawater temperature. To date, there are no direct estimates of the atmospheric CO_2 concentration for the Early and Middle Callovian. Yapp and Poths (1996) have suggested that the apparent Callovian atmospheric P_{CO_2} cannot be distinguished from a value equivalent to the modern CO_2 pressure, using C-isotope data from an $Fe(CO_3)OH$ component in oolitic goethites of Switzerland. Unfortunately, samples are only referred to as "Callovian" in age so that the precise sample position with respect to the severe early Late Callovian cooling is uncertain. Other Jurassic paleo-P_{CO_2} data inferred from $\delta^{13}C$ values of paleosol carbonates (Ekart and others, 1999; Ghosh

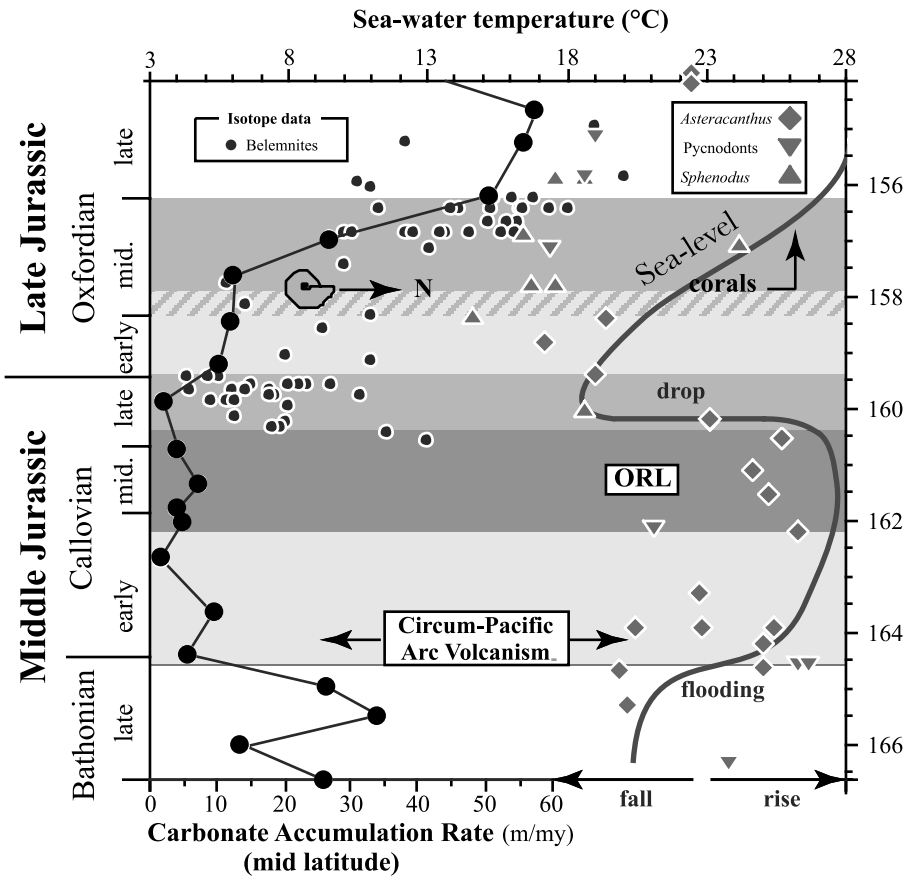

Fig. 5. Respective timing across the MLJT of carbonate accumulation rates, sea level, organic-rich sedimentation, circum-Pacific volcanism, and seawater temperatures. There was a pronounced cooling effect of the deposition of organic-rich sediments (Middle Callovian) via the excess uptake of C_{org} from the atmospheric CO_2 greenhouse gas. The carbonate minimum in the latest Callovian falls into the thermal minimum. Carbonate deposition increased after the thermal upgrading (early Middle Oxfordian, *vertebrale/antecedens* chrons) indicated by biogeographic data (ammonite and coral distribution).

and others, 2001) correspond to poorly age-controlled samples referred to as "Early", "early Middle" and "Late Jurassic". However, the occurrence of kaolinitic clays and ferruginous crusts/ooids in rather high-latitude Lower and Middle Callovian deposits in both hemispheres, up to 48°N in western Russia (Arkell, 1956) and 46°S in eastern Madagascar (Ranarison, ms, 1988) is suggestive of a CO_2-enriched paleoatmosphere (Thiry, 2000).

CO_2 outgassing by volcanoes.—Recent radiometric dating has documented extensive late Middle Jurassic subaerial volcanism in the circum-Pacific, prone to have delivered large amounts of CO_2 into the atmosphere. Arc volcanism was initiated in Patagonia (central Santa Cruz Province) and southeastern China (Hong Kong Province), at 164.1 Ma (Féraud and others, 1999) and 164.6 Ma (Davis and others, 1997) respectively, coincident in time with the sharp sea level rise around the Bathonian/Callovian transition at 164.4 Ma (Gradstein and others, 1994).

The Jurassic volcanic province of Patagonia in southern South America represents one of the largest silicic igneous provinces in the world, in association with a

half-graben type continental disruption behind a magmatic arc whose length attained at least 1,500 kilometers (Féraud and others, 1999). In the central Santa Cruz Province, the volcanic rocks of the *Bahia Laura Group* have yielded a cluster of radiometric dates ranging from 164.1 ± 0.3 to 157.9 ± 0.5 Ma (Ar/Ar dating; Féraud and others, 1999), that is earliest Callovian to earliest Middle Oxfordian. The volcanic rocks consist of rhyolitic/ignimbritic units that dominate over andesitic lava-flows. The thickness of the volcanic formation seen in the subsurface attains 2.2 kilometers. In the Patagonian Cordillera, for example the Lake Fontana area, the *El Quemado Complex* whose thickness ranges from nil to 2.1 kilometers, consists of an accumulation of porphyrites, rhyodacites, andesites, breccias and tuffs directly overlain by marine reefal limestone of the *Cotidiano Fm* (Riccardi, 1983) which can be assigned to the Middle Oxfordian (*plicatilis* Zone) by regional correlation with the *La Manga Fm* of the Bardas Blanca Area of the Neuquen Province (Legarreta, 1991). In the Chubut Province (central-west Patagonia), the *Lonco Trapial Group*, whose thickness exceeds 1.0 kilometer, is composed of porphyrites and tuffs intercalated with sandstones and conglomerates. It is overlain by a lacustrine formation referred to as *Canadon Asfalto Fm* (Riccardi, 1983), similarly dated as Middle Oxfordian *via* regional correlation. In the Far-South, the volcaniclastic suite of tuffs, tuffaceous sandstones, and rhyolites, referred to as *Tobifera Fm*, has been penetrated by both onshore and offshore exploratory oil wells, in Magallanes (Biddle and others, 1986) and western Malvinas (Galeazzi, 1998) basins, respectively. The total volcanic sequence reaches a maximum thickness of some 1.5 kilometers within deepest half-grabens, but is absent over basement highs. The upper *Tobifera Fm* has been assigned to the uppermost Middle Jurassic – Lower Callovian on the basis of outcrop dates (Biddle and others, 1986).

In northeast Asia, a belt of intrusive and extrusive rocks passes through the maritime provinces of eastern China and goes up to the Tajgonos Peninsula in eastern Russia (Shu and others, 1989; Sey and others, 1992; Wang and others, 1992). This magmatism, covering more than 1 Mkm^2, was generated by the subduction of the Kula-Pacific Plate beneath the Eurasian Plate (Zhou and Lao, 1990). In the Hebei and Liaoning provinces of northeastern China, the Bathonian-Callovian consists of a 500-meter thick sequence of andesitic tuffs and breccias sandwiched between fluvial deposits. In the Guangdong province of southern China, a thick (2–2.5 km) series of pyroclastic rocks, interbedded with lacustrine deposits, lies unconformably on the Lower Jurassic. Consistently, radiometric dates (U/Pb) obtained from Mesozoic granitoid rocks and volcanic formations of this district have yielded an early period of volcano-plutonism spanning from 164.6 ± 0.2 to 159.3 ± 0.3 Ma (Davis and others, 1997), that is latest Bathonian to earliest Oxfordian, and a second episode occurring much latter during the Middle Tithonian.

Additional subaerial volcanism only referred to as "late Middle Jurassic" in age has been documented in the circum-Pacific: northwestern Mexico (Baja California Peninsula; Salvador and others, 1992), Indonesian Borneo (Kalimatan Island; Sukamto and Westermann, 1992), northwestern Australia (Browse Basin; Stagg and Exon, 1981), and northeastern Australia (Cape York; Bradshaw and Challinor, 1992).

It is apparent that a large amount of intermediate-silicic rocks and gases, including CO_2, were probably supplied to surface environments by arc volcanoes of the Pacific during late Middle Jurassic times. However, the question of how much and how fast CO_2 entered the atmosphere *via* Jurassic circum-Pacific volcanic plumes is difficult to assess because estimates of the C flux from modern arc volcanoes vary considerably (0.4 to 3.3 10^{12} CO_2 mol/a; Marty and Tolstikhin, 1998) and the number of volcanoes in the Jurassic igneous provinces of the Pacific is unknown. The MORB contribution, for example in western Tethys (Brunn and others, 1970) and incipient Central Atlantic Ocean (Ogg and others, 1983), is not considered significant because the basaltic

magma generated at submarine ridges typically has very low volatile contents and the high water pressure at depth of eruption inhibits degassing of volatiles (Sparks and others, 1997).

Gas-hydrate dissociation.—Recent suggestions by Hesselbo and others (2000) and Bains and others (2000) for the Toarcian "Oceanic Anoxic Event" and Paleocene/Eocene Transition, respectively, that massive volcanism could have led to environmental changes sufficient to cause destabilization (and oxidation) of sea-floor gas-hydrate accumulations prompt us to investigate this possibility. Supporting evidence for such a contribution during Middle Callovian times might come from somewhat depleted ^{13}C values of both total organic carbon and terrestrial wood debris in the *Peterborough Mb* (Kenig and others, 1994), in coincidence with the maximal warming (fig. 4). However, certain geochemical data and geological observations contradict the hypothesis of gas hydrate release. First the coeval carbonate C-isotope data do not display any negative excursion (fig. 1). Second the amplitude of the negative excursion in organic matter is limited (~ -2 ‰) and the value for terrestrial primary biomass is not so severely depressed (-23.5 ‰) (Kenig and others, 1994). Third the trade-off between increasing temperature and increasing pressure (increasing water-depth from global sea level rise) trends we observe for the Middle Callovian (see above) would tend to stabilize marine gas hydrates (Paull and others, 1991; Kvenvolden, 1998). Fourth the Middle Callovian isotopic anomaly and warming lasted over ~2 my, a very long time interval for such a mechanism compared to the 10 ky of the "Latest Paleocene Thermal Maximum" episode (Dickens, 2000).

We conclude that arc-volcanic outgassing that was initiated in the Late Bathonian around the Pacific probably contributed to increase the concentrations of the greenhouse gas carbon dioxide during Early and Middle Callovian times, leading to a thermal optimum of seawater and an eustatic sea level rise.

Inverse Effect

MLJT climatic deterioration.—The temperature decline that occurred in the early Late Callovian, *athleta* Zone, just post-dated massive deposition of organic carbon (fig. 4). According to the time scale of Gradstein and others (1994), there is a time-gap of about 0.8 my between the termination of the organic rich-deposition in central England (*phaeinum/proniae* Subzone boundary) and sea level minimum (*henrici/lamberti* Subzone boundary). This lag-time that corresponds to the time required to build continental ice sheets may have been much shorter (0.2-0.3 my) if we consider that organic-rich sedimentation ceased at the end of *athleta* Zone in central Arabia (Hirsch and others, 1998).

This climatic deterioration that induced the migration of boreal fauna into low-latitude seas and forced the probable growth of continental ice around the MLJT can be ascribed to a downdraw in atmospheric CO_2 via enhanced organic-carbon burial, which acted as a negative feedback effect, which is an inverse Greenhouse Effect (Dromart and others, 2003). Cases for which some evidence of climatic cooling or simple termination of global warm periods are associated with organic-rich deposits and/or anomalous C-isotope records, are recurrent throughout the Earth's history, for example Neoproterozoic (Kaufman and others, 1997), Toarcian (Jenkyns and Clayton, 1997), Early/Late Valanginian (Reboulet and Atrops, 1995; Weissert and others, 1998; Pucéat and others, 2003), Aptian (Weissert and Lini, 1991), Cenomanian/Turonian (Arthur and others, 1988; Jenkyns and others, 1994), Paleocene/Eocene (Bains and others, 2000), Miocene (Vincent and Berger, 1985).

Jurassic CO_2 levels.—The severe refrigeration that affected the Earth for about 2 my around the MLJT implies that Jurassic atmospheric CO_2 levels might have been intermittently very low, that is lower than 500 ppmV. This proposition conflicts with the statement by Ekart and others (1999) that CO_2 levels were maintained at approxi-

mately 3000 ± 1000 ppmV throughout the Jurassic. The possible failure to detect low CO_2 levels from paleosol analyses may lie in a sampling bias in that calcretes preferentially form under warm conditions and the likelihood of preservation of the continental deposits in the stratigraphic record is much higher during periods of sea level rise (Cross, 1988). Real atmospheric CO_2 trends at the MLJT transition might possibly be estimated from the comparison of the $\delta^{13}C$ of coeval marine organic carbon and carbonates (Pagani and others, 1999).

PERTURBATION OF THE CARBONATE CYCLE

Chemical weathering of silicate and carbonate rocks converts CO_2 into dissolved HCO_3^- that is transferred to the oceans by rivers and precipitated there as carbonate minerals (calcite, aragonite, dolomite). These reactions tell us that the net result of Ca/Mg silicate weathering is the transfer of carbon from the surface system to buried carbonate rocks, whereas the transfer of carbon from Ca/Mg carbonate weathering is theoretically negligible because, on a million year time-scale, carbonate weathering is rapidly followed by equivalent carbonate deposition. These reactions also predict that any addition of CO_2 to the atmosphere should have, directly and by means of the atmospheric greenhouse effect that brings about higher global temperatures, an accelerating effect on both global weathering rates (Walker and others, 1981), and the precipitation of marine carbonates within a short delay of 0.01-1 my (Albarède, 1996; Berner, 1998).

Three stages have been distinguished in global carbonate sedimentation around the MLJT: 1) for the latest Bathonian to Middle Callovian, a withdrawal by drowning of shallow carbonate platforms from subtropical latitudes and a correlative enhancement of the neritic carbonate sedimentation over intertropical zones; 2) for the latest Callovian to Early Oxfordian, a widespread and pronounced decline of the carbonate sedimentation; 3) during the Middle Oxfordian, a general and abrupt recovery of carbonate platforms in terms of places and accumulation rates. In the following, the evolution of carbonate sedimentation is interpreted by comparing the data relative to contemporary Jurassic changes in the global environment.

The gradual and general drowning of the subtropical carbonate platforms from the latest Bathonian till the Middle Callovian is associated with subaerial volcanic outgassing and global sea level elevation (table 3). The correlation with volcanic degassing is somewhat paradoxical. If high $[CO_{2(atm)}]$ can reduce temporarily the biogenic calcification by lowering seawater pH (Riebesell and others, 2000), geochemical and mass balance models predict that any CO_2 addition into the atmosphere should have a positive impact on carbonate depositional systems in the following 0.01-1 my. This is because seawater alkalinity is raised in the process of enhanced weathering of continental silicate and carbonate rocks and a large amount of calcium is driven to the sea.

Subtropical platform drowning can be simply viewed as a result of the increase in water-depth that caused the benthic carbonate skeletal production to decrease (Sarg, 1988). However, the correlative deposition of carbonate-depleted sediments in outer-shelf environments of the Subalpine Basin of France (Elmi, 1967; Olivero and Atrops, 1996) and in the deep-water basins of the western Tethys (Baumgartner, 1984) suggests that sea level elevation by itself cannot be directly responsible for this gradual decline of the carbonate sedimentation. In fact, there is no reason why sediment production by the pelagic biota (pelecypods and phytoplankton) of distal environments should have been sensitive to any change of the water-column height.

The general decline of carbonate sedimentation in subtropical areas is here interpreted as a consequence of contemporary development of low-latitude carbonate platforms. Middle Callovian reefal platforms blossomed in northeastern Africa in response to the flooding of large epicontinental areas by shallow seas (table 1). Since

tropical reef communities are very prone to optimize the harvest of calcium carbonate from supersaturated waters (Wood, 1999), it is believed that low-latitude reefal platforms constituted the principal sink for the global carbonate sediment budget so that the Bathonian and Lower-Middle Callovian intervals mainly differ in the partitioning of carbonate masses between middle and low latitudes (fig. 1), without any detectable evolution in the overall global budget.

By contrast, carbonate depositional rates collapsed during the Late Callovian (fig. 1), after the organic pump had drawn down atmospheric CO_2, and while the eustatic sea level was low and continental ice caps were presumably present. This response is coherent with the geochemical and mass balance models that predict that any CO_2 subtraction from the atmosphere has a delayed negative impact on carbonate depositional systems. Thereby, it is suggested that the increase of the HCO_3^- flux related to shelf exposure has been totally overwhelmed by the detrimental impact on continental weathering of the observed temperature drop and the presumed [$CO_{2(atm)}$] decrease. The negative effect of low atmospheric CO_2 levels on the carbonate depositional budget is thought to have been long and pronounced around the MLJT because mountain belts were of such limited extent at this time (Ronov, 1994), knowing that chemical weathering is regularly sustained by mechanical denudation of continental rocks (Gaillardet and others, 1999a, 1999b). Supporting evidence that major topographic relief was globally quite limited comes from the seawater Sr-isotope curve whose Phanerozoic minimum occurs around the MLJT (see Veizer and others, 1999).

The long-term (~2 my) but slow improvement of carbonate sedimentation through Early and early Middle Oxfordian times (fig. 1) is suggestive of a self-recovery process of the carbonate cycle subsequent to atmospheric CO_2 buildup during glacial times. The subsequent steep rise in carbonate sediment production during the Middle Oxfordian was associated with warming and onset of aridity in mid- to high-latitudes: northern Europe (Abbink and others, 2001) and Central Asia (Ritts and others, 1999). However, the temperature elevation in western Europe at *vertebrale/antecedens* Subzones boundary anticipated the massive and widespread deposition of carbonates (lower *transversarium* Zone) by about 0.8 myr (fig. 5), so that the Middle Oxfordian enhanced carbonate precipitation turns out to be a consequence, and a contribution to, rather than a cause of climate modification. Although we do not develop what triggered climatic change, several scenarios are explored that can account for the subsequent boost of global carbonate sedimentation.

According to the model proposed by Kennedy and others (2001) for the Neoproterozoic postglacial *Cap Carbonates*, the warming and flooding of widely exposed continental shelves accompanying any postglacial transgression would destabilize permafrost gas hydrate, and stimulate the carbonate cycle. Notably, negative $\delta^{13}C_{car}$ values have been found in Oxfordian fine-grained limestones of the Subalpine basin in southeastern France: Uppermost Lower Oxfordian (*cordatum* Zone) in the Beauvoisin section by Gaillard and others (1992) and Middle Oxfordian (*plicatilis/transversarium* Zone transition) in the Vergons section by Padden and others (2001). The strongly ^{13}C-depleted values from - 24.6 to 9.7 permil of the massive and nodular limestones of the Beauvoisin section have been related to cold hydrocarbon seeps (Gaillard and others, 1992). Similarly, the coupled C_{inorg} / C_{org} negative excursion in the Vergons section has been interpreted to be derived from a sudden release of methane from buried gas hydrates (Padden and others, 2001). However, these negative $\delta^{13}C$ values appear to be both spread out in time and associated with local submarine release of methane because analyses from time-equivalent series, that is *plicatilis/transversarium* Zone transition, located all around the Subalpine basin [Chabrières, Aubenas, Pery-Reuchenette sections, appendix D (table D1 and D2)] record no negative $\delta^{13}C_{car}$ values. So, to date, with the general absence of negative carbon isotopic signatures in

the Middle Oxfordian limestones, the hypothesis of massive and general gas hydrate dissociation a priori cannot be retained here.

Alternatively, post-glacial continental ice melting and withdraw induced lithospheric rebound, but no evidence of enhanced crustal weathering rates is apparent in Oxfordian-Kimmeridgian Sr isotopic data (*in* Jenkyns and others, 2002). The remaining possibility is that the known connection, that developed at this time, between the equatorial Pacific and Tethys seawaters (fig. 2) modified the general oceanic and atmospheric circulation, causing changes to the global runoff distribution and an increase of the HCO_3^- production rate by continental weathering. Buffering of the strontium isotopic ratio by enhanced carbonate weathering and dissolution provides one possible explanation for the lack of its variation.

SUMMARY AND CONCLUSIONS

The geological and geochemical data presented here show how certain components of the global environment, such as carbonate platforms, sea level, seawater temperature and chemistry, responded to a probable extra addition of CO_2 into the atmosphere by volcanic degassing. A prominent impact of this natural perturbation consisted of a general drop of the carbonate sedimentation associated with a severe refrigeration of the Earth's surface at the Middle/Late Jurassic Transition, which is the Callovian/Oxfordian boundary. As to the mechanisms involved in this somewhat paradoxical effect on the carbon cycle and global environment, the conclusions are as follows.

Jurassic Climate Regulation

The general, abrupt and pronounced cooling which followed enhanced organic-carbon sequestration during the Late Callovian supports the general assumption that Jurassic Earth's surface temperatures were controlled by the abundance of CO_2 in the atmosphere. The severe refrigeration recorded at the MLJT suggests that Mesozoic CO_2 levels could have dropped to values lower than 500 ppmV for short periods.

Carbonate Budget and Partitioning

Reefal carbonate platforms thrived over intertropical latitudes throughout Middle Callovian times, owing to a major eustatic sea level rise. The enhanced production of carbonate sediments at low latitudes is believed to have caused a drop of carbonate sediment production at higher latitudes (drowning of Bathonian – L. Callovian subtropical platforms).

It should be noted that the latitudinal constriction of the carbonate platforms conventionally referred to as "tropical" and "warm" paradoxically coincided in time with a rise of the upper seawater temperatures, and that this shift in carbonate sedimentation towards low latitudes apparently did not modify the global carbonate sedimentation budget. Conversely, the [$CO_{2(atm)}$] drop and climatic deterioration during the Late Callovian lowered the overall carbonate sediment production. The detrimental effect of climatic changes on the carbonate cycle is thought to have been quite marked because continental topographic components were apparently very minor at this time.

The overlying, post-glacial Middle Oxfordian carbonates share a similar stratigraphic order with the Neoproterozoic *Cap carbonates* and the Holocene neritic carbonates. The reason why the carbonate platforms and surface temperatures recovered through Oxfordian times is not totally understood. The initial, gradual recovery of the carbonate sedimentation picked up sharply during the Middle Oxfordian, apparently post-dating the thermal rise of the western Tethys seawaters.

Linkage of C_{org} and C_{inorg} Cycles

Periods of intensified C_{org} burial were coupled with enhanced C_{inorg} burial on carbonate platforms (Middle Callovian, Middle Oxfordian), and coincident with eustatic transgressive conditions and thermal optima of surface seawaters. Reciprocally, times of reduced C_{org} burial were correlated with periods of very limited carbonate precipitation (Late Callovian to Early Oxfordian), coinciding with a major sea level lowstand and cool conditions. Throughout the non-glacial episodes, combined high [$CO_{2(atm)}$] and surface temperatures favored the production/preservation of organic-rich deposits, and continental weathering. Conversely, throughout the glacial episode, organic matter was oxidized in cool marine waters, and the global HCO_3^- flux was reduced in response to low atmospheric CO_2 levels. For the Jurassic, the C_{org} and C_{inorg} cycles were linked, and the mechanisms that underlined this linkage were related to the overall correlation existing between atmospheric CO_2 concentration and surface temperature.

General Model

The model explains how and why the carbonate-free and frosted Earth response to some extra aerial volcanic activity was delayed by several million years. By contrast, the way out of this extreme situation is not resolved and, in particular, we ignore whether the carbonate cycle was able to recover by itself or was stimulated by any geodynamic event. The course of the Mesozoic was marked by a number of events associating subaerial volcanism (Large Igneous Provinces), global anoxia, carbonate dearth, and cool conditions. That is the case at least for the Early Toarcian, the Early/Late Valanginian transition, the Early Aptian, the Cenomanian/Turonian transition, the K/T transition. A similar integrative description of these events should enable the MLJT scenario to be tested and refined. We anticipate that the inverse greenhouse effect was something common even if its impact on the surface environments was variable. We presume also that the detrimental, long-term effect of subaerial volcanic outgassing on carbonate sedimentation is likely to be very specific to the Jurassic because of a very smoothed morphology of Earth at this time.

ACKNOWLEDGMENTS

Samples from Central Atlantic were provided by Ocean Drilling Program, and organic carbon analyses (pyrolysis) were carried out at the Institut Français du Pétrole. We thank G. Sambet (Elf France), F. Guillocheau (Rennes 1), P. Plummer (Seychelles NOC), L. Jansa and J. Christopher (GS Canada) for much help in collecting well data, M. Philippe and S. Elmi (Lyon) for providing bibliography, and D. Goujet (MNHN, Paris), A. Léna and G. Gallio (MHN, Besançon), J. H. Delance (University of Burgundy, Dijon), Museum of Lausanne via M. Weidmann for provision of vertebrate samples. Oxygen- and carbon-isotope analyses were carried out at the ENS, Lyon and MIT, Cambridge. Scientific discussion with F. Albarède, P. Amiotte-Suchet, J. Grotzinger, and A. Knoll is gratefully acknowledged. M. Pagani, S. Hesselbo, and H. Weissert provided constructive remarks through their review. This work was supported by the French INSU-CNRS Program *Intérieur de la Terre* "Comportement dynamique des plates-formes carbonatées".

APPENDIX A

TABLE A1

Upper Middle and lower Upper Jurassic stratigraphic subdivisions

Time (Ma)[1]	Stage	Substages	ASZ (zones)[2]	ASZ (subzones)[2]
154.1	Kimmeridgian		Platynota	
	Oxfordian			Galar
			Planula	Planula
				Hauffianum
				Bimammatum
				Berrense
			Bimammatum	Semimammatum
				Grossouvrei
		Upper	Bifurcatus	Stenocycloïdes
				Rotoïdes
				Schilli
				Luciaeformis
			Transversarium	Parandieri
				Antecedens
		Middle	Plicatilis	Vertebrale
				Cordatum
				Costicardia
			Cordatum	Bukowski
				Praecordatum
159.4	Oxfordian	Lower	Mariae	Scarburgense
	Callovian			Lamberti
			Lamberti	Henrici
				Spinosum
				Proniae
		Upper	Athleta	Phaeinum
				Grossouvrei
			Coronatum	Obductum
				Jason
		Middle	Jason	Medea
				Enodatum
			Calloviense	Calloviense
				Galilei
				Curtilobus
			Koenigi	Gowerianus
				Kamptus
				Terebratus
164.4	Callovian	Lower	Herveyi	Keppleri
	Bathonian			Discus
			Dicus	Hollandi
				Hannoveranus
				Julii
			Retrocostatum	Densicostatum
				Fortecostatum
		Upper	Bremeri	Bullatimorphus
			Morrisi	Morrisi
			Subcontractus	Subcontractus
				Progracilis
		Middle	Progracilis	Orbignyi
				Tenuiplicatus
				Yeovilensis
				Macrescens
169.2	Bathonian	Lower	Zigzag	Convergens

(1) Timescale by Gradstein and others, 1994
(2) ASZ: Ammonite Standard Zonation; Bathonian: Mangold and Rioult, 1997; Callovian: Thierry and others, 1997; Oxfordian: Cariou and others, 1997

APPENDIX B

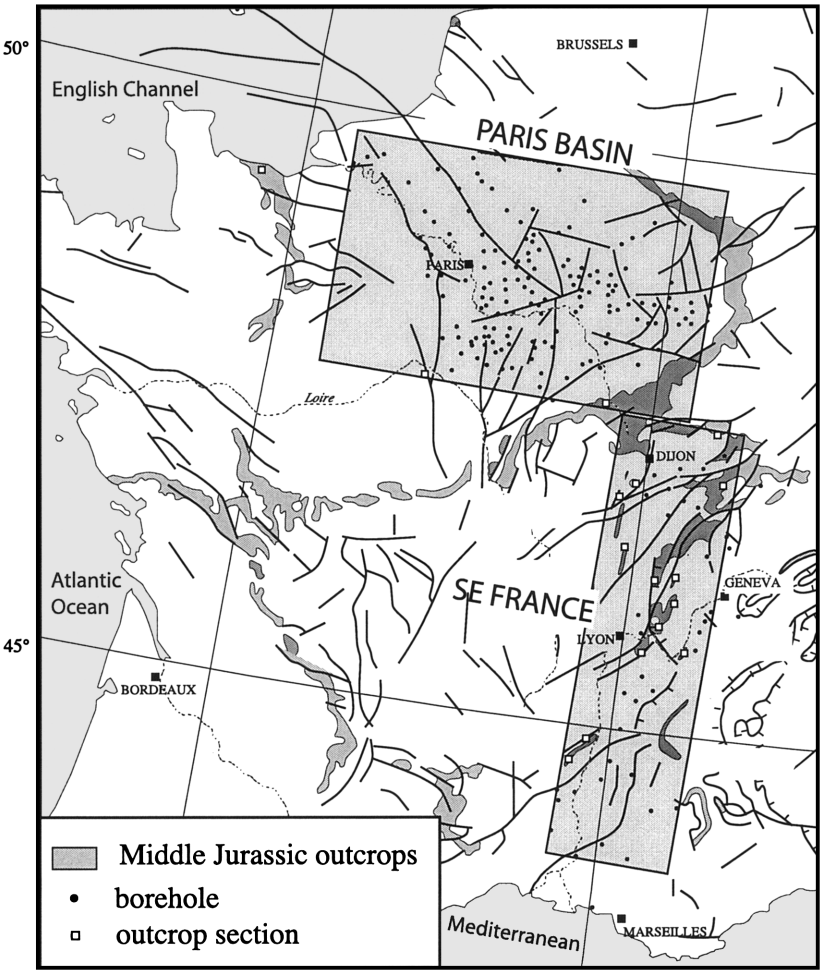

Fig. B1. Areas of France (Paris Basin and southeastern France) over which Middle and Upper Jurassic carbonate accumulation rates have been calculated (table B1 ; fig. 1)

TABLE B1

Calculated values of Middle and Upper Jurassic carbonate accumulation in the Paris Basin and eastern France, respectively (fig. 1)

Basin	Surface (km^2)	Well Control	Stratigraphy	Interval Boundary	Age (Ma)	Duration (My)	Volume (km^3)	Thickness (m)	3D rate (m/My)
				Beckeri/Hybonotum Z					
East France	44, 340	78	U. Kimmeridgian		151.5	1.2	1725.8	38.92	32.43
				Acanthicum/Eudoxus Z					
East France	44, 120	82	U. Kimmeridgian		152.6	1	1274.2	28.88	28.88
				Hypselocyclum/Divisum Z					
East France	44, 120	79	L. Kimmeridgian		153.65	1.1	1564.2	35.46	32.24
				Platynota Sz					
East France	46, 060	78	Oxf./Kimmerid.		154.6	0.8	2112.2	45.86	57.32
				Haufianum Sz					
East France	46, 290	79	U. Oxfordian		155.2	0.8	2051.4	44.32	55.4
				Semimammatum Sz					
East France	45, 810	89	M.-U. Oxfordian		156.15	1.1	2536.2	55.36	50.33
				Luciaeformis/Schilli Sz					
East France	44, 350	99	M. Oxfordian		156.95	0.5	592.83	13.37	26.74
				Plicatilis/Transversarium Z					
East France	44, 350	102	M. Oxfordian		157.6	0.8	432.89	9.76	12.2
				Cordatum/Plicatilis Z					
East France	44, 330	98	L. Oxfordian		158.4	0.8	423.38	9.55	11.94
				Mariae/Cordatum Z					
East France	44, 330	98	U. Call.- L. Oxf.		159.2	0.8	363.57	8.2	10.25
				Lamberti Z (MB 34)					
Paris Basin	82, 875	164	U. Callovian		159.85	0.9	125.14	1.51	1.68
				Athleta Z (MB 33)					
Paris Basin	82, 875	164	M.-U. Callovian		160.7	0.8	252.77	3.05	3.81
				Oxoniensis BMB 32					
Paris Basin	82, 875	164	M. Callovian		161.3	0.4	238.68	2.88	7.2
				Jason Z (MB 29)					
Paris Basin	82, 875	164	M. Callovian		161.75	0.3	90.33	1.09	3.63
				Orbignyana BMB 28					
Paris Basin	82, 875	164	M. Callovian		162	0.4	147.52	1.78	4.44
				Torqui BMB 27					
Paris Basin	82, 875	164	L. Callovian		162.65	1.1	135.92	1.64	1.49
				Kalli BMB 26					
Paris Basin	82, 875	164	L. Callovian		163.6	0.6	453.33	5.47	9.12
				Divio BMB 24					
Paris Basin	82, 875	164	U. Bath.-L. Call.		164.35	0.7	318.24	3.84	5.48
				Eudesia BMB 23					
Paris Basin	82, 875	164	U. Bathonian		164.95	0.7	1496.72	18.06	25.81
				Digona BMB 20					
Paris Basin	82, 875	164	U. Bathonian		165.45	0.3	835.38	10.08	33.6
				Retrocostatum Z (MB 19)					
Paris Basin	82, 875	164	U. Bathonian		166	0.8	890.91	10.75	13.44
				Concinna BMB 18					
Paris Basin	82, 875	164	M. Bathonian		166.6	0.4	849.47	10.25	25.62
				Morrisi Z (MB 17)					
Paris Basin	82, 875	164	M. Bathonian		166.95	0.3	750.02	9.05	30.16
				Multiplicata BMB 16					
Paris Basin	82, 875	164	M. Bathonian		167.35	0.5	700.29	8.45	16.9
				Progracilis Z (MB 15)					
Paris Basin	82, 875	164	M. Bathonian		167.85	0.3	577.64	6.97	23.24
				Globata BMB 14					
Paris Basin	82, 875	164	L. Bathonian		168.15	0.5	546.15	6.59	13.18
				Yeovilensis Z (MB 12)					
Paris Basin	82, 875	164	L. Bathonian		168.55	0.3	827.92	9.99	33.31
				Macrescens Sz (MB 10)					
Paris Basin	82, 875	164	L. Bathonian		168.9	0.4	1633.47	19.71	49.27
				Convergens Sz (MB 5)					
Paris Basin	82, 875	164	U. Bajocian		169.25	0.3	357.19	4.31	14.38
				Bomfordi SZ (MB 3)					

BMB: Brachiopod Marker Bed (Garcia and Dromart, 1997)

Ages and durations inferred through report of biostratigraphic information into the time scale of Gradstein and others, 1994

Volumes of carbonate calculated according to the approach developed by Dromart and others (2002) (i.e. Inverse Distance Method)

Thickness: Average thickness of carbonate obtained by dividing the total volume of carbonate by the total surface

3D rate obtained by dividing the average thickness by the duration

TABLE B2

Comparative carbonate accumulation rates across Middle and Upper Jurassic contemporary tropical (Arabian Peninsula) and subtropical (western Europe) platforms (fig. 1)

Stratigraphic Interval	Transect location[1-2]	Min. Thickness[3] (m)	Max. Thickness[3] (m)	Duration[4] (m.yr.)	Min. Rate (m/m.yr.)	Max. Rate (m/m.yr.)	Average Rate (m/m.yr.)
	Arabian Peninsula[1]	58.8	63.23		13.8	16.2	
[Middle - Upper Oxfordian]				3.9			27.55
	W. Europe (E. France)[2]	146.09	166.65		37.5	42.7	
	Arabian Peninsula[1]	0	0		0	0	
[Upper Callovian - Lower Oxfordian]				3			4.55
	W. Europe (E. France)[2]	22.62	32.02		7.5	10.7	
	Arabian Peninsula[1]	88.25	149.9		26.1	44.1	
[Lower - Middle Callovian]				3.4			21.8
	W. Europe (E. France)[2]	25.4	32.95		7.5	9.7	
	Arabian Peninsula[1]	81.6	150.7		17	31.4	
[Bathonian]				4.8			28.15
	W. Europe (E. France)[2]	128.36	180.2		26.7	37.5	
(1) Arabian Peninsula (770 km)	Khashm adh Dhibi (SA)	Dukhan (Quatar)	Well A (U.A.E)	Well D (U.A.E.)			
	24° 11' 19" N	25° 30' 25" N	25° 28' 52" N	25° 29' 37" N			
	46° 18' 50" E	50° 47' 44" E	52° 51' 33 "E	54° 19' 26 ' E			
			Maydam Mahzan Field	Fateh Field			
(2) East France (wells) (685 km)	A 801	HTM 102	Lo.1	CMZ	Fa. 1	Ang.1	
	49° 41' 40" N	48° 26' 53" N	47° 06' 03" N	43° 58' 27" N	45° 23' 24" N	43° 57' 47" N	
	04° 00' 23" E	05° 22' 58" E	05° 15' 45" E	05° 17' 45" E	05° 09' 54" E	04° 46' 17" E	

(3) calculated carbonate thickness according to the procedure by Dromart and others, 1996

(4) according to the Jurassic timescale by Gradstein and others, 1994

APPENDIX C

Table C1

Pyrolysis data for Middle-Upper Jurassic sediments of DSDP site 534, Central Atlantic (fig. 4)

Sub-unit 534A	Position core/section/cm	Sub-bottom Depth (m)	Stratigraphy	Sediment	T.O.C. %	Tmax °C	IH (mgHC/gTOC)
7a	112/1/106*	1505.56	Oxfordian	claystone	0.2€		0
7a	115/1/34	1531.84	Oxfordian	dark reddish claystone	0.03		
7a	115/1/36	1531.86	Oxfordian	olive greenish claystone	0.02		
7a	115/1/38	1531.88	Oxfordian	dusky reddish claystone	0.02		
7b	119/1/111	1579.61	Oxfordian (base)	olive greenish claystone	0.15	423	46
7b	119/1/120	1579.70	Oxfordian (base)	black claystone	0.03		
7c	122/1/14**	1590.14	Callovian/Oxfordian	marly limestone (turbiditic)	0.38		
7c	122/1/35*	1590.35	Callovian/Oxfordian	marly limestone (turbiditic)	0.5€	429	70
7c	122/2/46	1591.96	Upper Callovian	dark greenish, silty claystone	0.49	429	106
7c	123/2/79**	1592.29	Upper Callovian	marly limestone (turbiditic)	0.47		
7c	123/2/99**	1592.49	Upper Callovian	dark claystone	1.30		
7c	123/3/20*	1597.20	Upper Callovian	calcareous silty claystone	0.9€	429	102
7c	124/1/59*	1604.09	Middle/Upper Callovian	marly limestone (turbiditic)	0.4€	433	83
7c	125/2/29	1614.29	Middle Callovian	dark greenish, silty claystone	1.97	435	186
7c	125/2/100*	1615.00	Middle Callovian	dark greenish claystone	1.8€	431	161
7c	125/3/100**	1616.5	Middle Callovian	black claystone	1.8		
7d	125/4/70**	1617.70	Middle Callovian	black claystone	2.40		
7d	125/5/44	1618.94	Middle Callovian	dark greenish claystone	3.31	433	226
7d	125/6/40	1620.40	Middle Callovian	black greenish claystone	3.28	434	237
7d	126/2/30**	1623.36	Middle Callovian	calcareous claystone	1.10		
7d	126/2/76*	1623.76	Middle Callovian	claystone	3.09€	430	221
7d	126/2/118	1624.18	Middle Callovian	dark greenish claystone	2.68	435	205
7d	126/3/16	1624.66	Middle Callovian	dark greenish claystone	1.44	434	60
7e	126/4/20	1626.20	Middle Callovian	calcareous claystone	0.16		
7e	127/1/05	1630.55	Middle Callovian	dark brownish claystone	0.11	420	63
7e	127/1/120	1631.70	Middle Callovian	dark greenish claystone	1.06	432	117
7e	127/1/130	1631.80	Middle Callovian	black claystone	1.29	434	121
7e	127/2/36	1632.36	Middle Callovian	dark greenish claystone	0.4	428	100
7e	127/2/37	1632.37	Middle Callovian	black, mm-thick lamina	3.11	432	270
7e	127/2/42	1632.47	Middle Callovian	dark brownish claystone	0.05	434	20
7e	127/3/74	1634.24	Middle Callovian	dark greenish claystone	0.35	426	94

*Data from Herbin and others (1983)
**Data from Sheridan and Gradstein (1983)
Stratigraphy based on dinoflagellates (Habid and Drugg, 1983)
Rock-Eval pyrolysis data obtained at Institut Français du Pétrole
T.O.C.: Total Organic Carbon (€: LECO Analysis)
Tmax: Pyrolysis thermal maximum, *i.e.* thermally immature organic matter (Tmax < 435°C)
IH: Pyrolysis Hydrogen Index, *i.e.* mixture of continental (IH < 100) and marine (IH > 100) organic matter

APPENDIX D

TABLE D1

Bulk carbon and oxygen isotope composition of Middle-Upper Jurassic carbonate rocks in western Europe (East France, Switzerland) (fig. 1)

Location	Stratigraphy	Standard Zonation		Age	Lithology	$\delta^{18}O$	$\delta^{13}C$
		(ammonite zones)	(ammonite subzones)	(Ma)		‰, PDB	‰, PDB
Ardèche, Aubenas (FR)	U. Oxfordian	Planula	Planula	154.6	Mudstone	-2.91	2.81
Ardèche, Aubenas (FR)	U. Oxfordian	Planula	Planula	154.7	Mudstone	-3.05	2.74
Ardèche, Aubenas (FR)	U. Oxfordian	Bimammatum	Hauffianum	154.8	Mudstone	-3.14	2.69
Ardèche, Aubenas (FR)	U. Oxfordian	Bimammatum	Hauffianum	154.8	Mudstone	-3.48	2.79
Ardèche, Aubenas (FR)	U. Oxfordian	Bimammatum	Hauffianum	154.8	Mudstone	-3.09	2.78
Ardèche, Aubenas (FR)	U. Oxfordian	Bimammatum	Hauffianum	154.9	Mudstone	-3.34	2.48
Ardèche, Aubenas (FR)	U. Oxfordian	Bimammatum	Hauffianum	154.9	Mudstone	-3.55	2.39
Ardèche, Aubenas (FR)	U. Oxfordian	Bimammatum	Bimammatum	155.0	Mudstone	-3.50	2.66
Ardèche, Aubenas (FR)	U. Oxfordian	Bimammatum	Bimammatum	155.0	Mudstone	-3.41	2.51
Ardèche, Aubenas (FR)	U. Oxfordian	Bimammatum	Bimammatum	155.1	Mudstone	-3.64	2.87
Ardèche, Aubenas (FR)	U. Oxfordian	Bimammatum	Bimammatum	155.1	Mudstone	-3.72	2.79
Ardèche, Aubenas (FR)	U. Oxfordian	Bimammatum	Bimammatum	155.2	Mudstone	-3.76	2.62
Ardèche, Aubenas (FR)	U. Oxfordian	Bimammatum	Berrense	155.3	Mudstone	-3.53	2.59
Ardèche, Aubenas (FR)	U. Oxfordian	Bimammatum	Semimammatum	155.4	Mudstone	-3.63	2.53
Ardèche, Aubenas (FR)	U. Oxfordian	Bimammatum	Semimammatum	155.4	Mudstone	-4.11	2.71
Ardèche, Aubenas (FR)	U. Oxfordian	Bimammatum	Semimammatum	155.5	Mudstone	-4.05	2.41
Ardèche, Aubenas (FR)	U. Oxfordian	Bimammatum	Semimammatum	155.5	Mudstone	-3.33	2.60
Ardèche, Aubenas (FR)	U. Oxfordian	Bimammatum	Semimammatum	155.6	Mudstone	-3.42	2.61
Ardèche, Aubenas (FR)	U. Oxfordian	Bifurcatus	Grossouvrei	155.7	Mudstone	-3.63	2.64
Ardèche, Aubenas (FR)	U. Oxfordian	Bifurcatus	Grossouvrei	155.8	Mudstone	-2.69	2.75
Ardèche, Aubenas (FR)	U. Oxfordian	Bifurcatus	Grossouvrei	155.8	Mudstone	-3.68	2.86
Ardèche, Aubenas (FR)	U. Oxfordian	Bifurcatus	Grossouvrei	155.9	Mudstone	-3.67	2.89
Ardèche, Aubenas (FR)	U. Oxfordian	Bifurcatus	Stenocycloides	156.0	Mudstone	-2.90	2.77
Ardèche, Aubenas (FR)	U. Oxfordian	Bifurcatus	Stenocycloides	156.1	Mudstone	-3.45	2.65
Ardèche, Aubenas (FR)	U. Oxfordian	Bifurcatus	Stenocycloides	156.1	Mudstone	-3.01	2.63
Ardèche, Aubenas (FR)	M. Oxfordian	Transversarium	Rotoides	156.2	Mudstone	-3.63	2.44
Ardèche, Aubenas (FR)	M. Oxfordian	Transversarium	Schilli	156.3	Mudstone	-4.05	2.44
Ardèche, Aubenas (FR)	M. Oxfordian	Transversarium	Schilli	156.4	Mudstone	-3.33	2.43
Ardèche, Aubenas (FR)	M. Oxfordian	Transversarium	Luciaeformis	156.6	Mudstone	-3.22	2.51
Ardèche, Aubenas (FR)	M. Oxfordian	Transversarium	Luciaeformis	156.8	Mudstone	-3.45	2.46
Ardèche, Aubenas (FR)	M. Oxfordian	Transversarium	Parandieri	157.0	Mudstone	-2.77	2.90
Ardèche, Aubenas (FR)	M. Oxfordian	Transversarium	Parandieri	157.1	Mudstone	-3.57	2.41
Ardèche, Aubenas (FR)	M. Oxfordian	Plicatilis	Antecedens	157.4	Mudstone	-1.43	2.48
Pery-Reuchenette (CH)	U. Oxfordian	Bifurcatus	Stenocycloides	156.0	Mudstone	-2.97	2.28
Pery-Reuchenette (CH)	U. Oxfordian	Bifurcatus	Stenocycloides	156.0	Mudstone	-3.00	1.96
Pery-Reuchenette (CH)	U. Oxfordian	Bifurcatus	Stenocycloides	156.0	Mudstone	-3.71	2.09
Pery-Reuchenette (CH)	U. Oxfordian	Bifurcatus	Stenocycloides	156.1	Mudstone	-3.21	1.99
Pery-Reuchenette (CH)	U. Oxfordian	Bifurcatus	Stenocycloides	156.1	Silty Mudstone	-4.49	1.83
Pery-Reuchenette (CH)	U. Oxfordian	Bifurcatus	Stenocycloides	156.1	Silty Mudstone	-2.49	2.34
Pery-Reuchenette (CH)	U. Oxfordian	Bifurcatus	Stenocycloides	156.1	Silty Mudstone	-2.98	2.92
Pery-Reuchenette (CH)	U. Oxfordian	Transversarium	Rotoides	156.2	Mudstone	-3.09	2.62
Pery-Reuchenette (CH)	M. Oxfordian	Transversarium	Schilli	156.3	Mudstone	-3.64	2.81
Pery-Reuchenette (CH)	M. Oxfordian	Transversarium	Schilli	156.3	Mudstone	-3.18	2.64
Pery-Reuchenette (CH)	M. Oxfordian	Transversarium	Schilli	156.3	Mudstone	-4.25	2.57
Pery-Reuchenette (CH)	M. Oxfordian	Transversarium	Schilli	156.4	Mudstone	-2.71	2.27
Pery-Reuchenette (CH)	M. Oxfordian	Transversarium	Schilli	156.4	Mudstone	-3.06	2.10
Pery-Reuchenette (CH)	M. Oxfordian	Transversarium	Schilli	156.4	Mudstone	-2.22	2.44
Pery-Reuchenette (CH)	M. Oxfordian	Transversarium	Schilli	156.5	Mudstone	-3.18	2.64
Pery-Reuchenette (CH)	M. Oxfordian	Transversarium	Schilli	156.5	Mudstone	-3.17	2.75
Pery-Reuchenette (CH)	M. Oxfordian	Transversarium	Luciaeformis	156.6	Mudstone	-4.20	2.91
Pery-Reuchenette (CH)	M. Oxfordian	Transversarium	Luciaeformis	156.6	Mudstone	-3.81	3.14
Pery-Reuchenette (CH)	M. Oxfordian	Transversarium	Luciaeformis	156.7	Mudstone	-3.92	3.02
Pery-Reuchenette (CH)	M. Oxfordian	Transversarium	Luciaeformis	156.8	Mudstone	-3.09	3.21
Pery-Reuchenette (CH)	M. Oxfordian	Transversarium	Parandieri	156.9	Mudstone	-3.59	3.19
Pery-Reuchenette (CH)	M. Oxfordian	Transversarium	Parandieri	157.0	Mudstone	-3.87	3.07
Pery-Reuchenette (CH)	M. Oxfordian	Transversarium	Parandieri	157.1	Mudstone	-2.58	2.57
Pery-Reuchenette (CH)	L. Callovian			164.1	Packstone	-4.78	1.94
Pery-Reuchenette (CH)	L. Callovian			164.2	Grainstone	-5.05	2.00

Aubenas section stratigraphy by Atrops (unpublished data); ASZ: Ammonite Standard Zonation
Pery-Reuchenette section stratigraphy by Gygi (personal information)
Aubenas samples analyzed at E.N.S. Lyon, France
Pery-Reuchenette samples analyzed at M.I.T., MA, USA

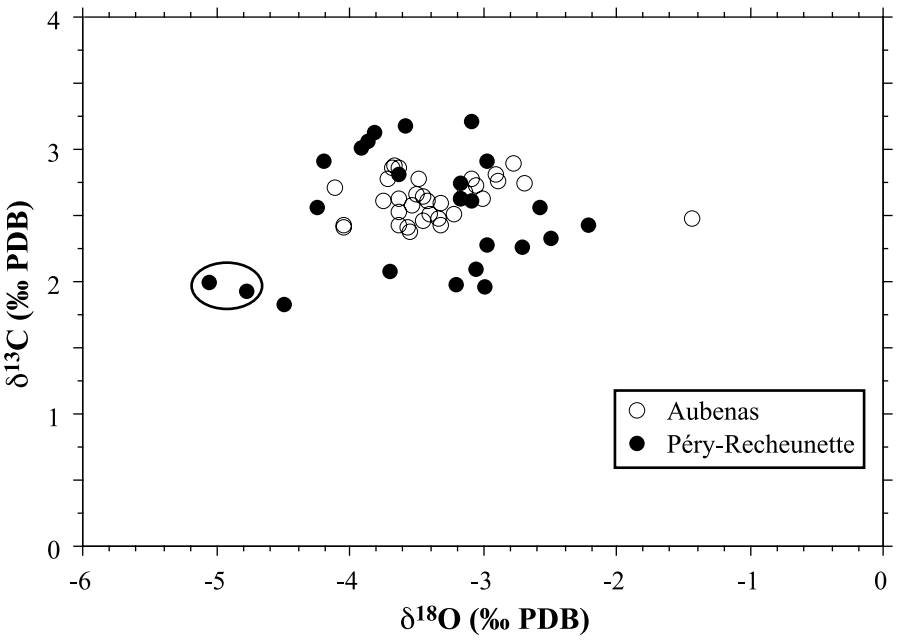

Fig. D1. $\delta^{13}C$ versus $\delta^{18}O$ for bulk Middle-Upper Jurassic carbonates in western Europe (table D1). Two samples from Péry-Reuchenette are grainstone/packstone considered to have been diagenetically altered (spar cements).

TABLE D2

Bulk carbon isotope composition of Middle-Upper Jurassic rocks in western Tethys (East France, Italy) (fig. 1)

Location	Lithology	Stratigraphy	Standard Zonation (ammonite zones)	Standard Zonation (ammonite subzones)	Age (Ma)	$\delta^{13}C$ ‰, PDB
Terminilletto (IT)	Cherty Mudstone	Kimmeridgian			153.6	2.3
Terminilletto (IT)	Cherty Mudstone	Kimmeridgian			153.7	2.4
Terminilletto (IT)	Cherty Mudstone				154.1	2.5
Terminilletto (IT)	Cherty Mudstone				154.6	2.6
Terminilletto (IT)	Cherty Mudstone	M-U. Oxfordian			155.4	2.5
Terminilletto (IT)	Cherty Mudstone	M-U. Oxfordian			155.6	2.4
Terminilletto (IT)	Cherty Mudstone	M-U. Oxfordian			155.8	2.6
Terminilletto (IT)	Cherty Mudstone	M-U. Oxfordian			156	2.5
Terminilletto (IT)	Cherty Mudstone	M. Oxfordian			156.4	2.8
Terminilletto (IT)	Cherty Mudstone	M. Oxfordian			156.6	2.9
Terminilletto (IT)	Cherty Mudstone	M. Oxfordian			156.8	3
Terminilletto (IT)	Cherty Mudstone				157	2.9
Terminilletto (IT)	Cherty Mudstone				152.2	2.8
Terminilletto (IT)	Cherty Mudstone				157.3	2.9
Terminilletto (IT)	Cherty Mudstone				157.4	3
Terminilletto (IT)	Cherty Mudstone				157.5	2.9
Terminilletto (IT)	Cherty Mudstone				157.6	2.9
Terminilletto (IT)	Cherty Mudstone				157.8	2.7
Terminilletto (IT)	Cherty Mudstone				158.0	2.5
Terminilletto (IT)	Cherty Mudstone				158.6	2.5
Terminilletto (IT)	Cherty Mudstone	L. Oxfordian			158.7	2.6
Terminilletto (IT)	Cherty Mudstone	L. Oxfordian			158.8	2.7
Terminilletto (IT)	Cherty Mudstone				159.0	2.9
Terminilletto (IT)	Cherty Mudstone				159.2	2.8
Terminilletto (IT)	Cherty Mudstone				159.8	3.1
Terminilletto (IT)	Cherty Mudstone				160.4	2.8
Terminilletto (IT)	Cherty Mudstone				160.8	3
Terminilletto (IT)	Cherty Mudstone	M. Callovian			161.0	3.2
Terminilletto (IT)	Cherty Mudstone	M. Callovian			161.2	3.1
Terminilletto (IT)	Cherty Mudstone	L. Callovian			161.8	3

TABLE D2
(continued)

Location	Lithology	Stratigraphy	Standard Zonation (ammonite zones)	Standard Zonation (ammonite subzones)	Age (Ma)	$\delta^{13}C$ ‰, PDB
Terminilletto (IT)	Cherty Mudstone	L. Callovian			162.4	3.2
Terminilletto (IT)	Cherty Mudstone	U. Bathonian			164.6	2.5
Terminilletto (IT)	Cherty Mudstone	U. Bathonian			165.4	2.3
Terminilletto (IT)	Cherty Mudstone	U. Bathonian			166	2.4
Terminilletto (IT)	Cherty Mudstone	M/U. Bathonian			166.8	2.3
Terminilletto (IT)	Cherty Mudstone	L-M. Bathonian			167	2.4
Terminilletto (IT)	Cherty Mudstone	L-M. Bathonian			167.4	2.5
Terminilletto (IT)	Cherty Mudstone	L-M. Bathonian			167.8	2.4
Terminilletto (IT)	Cherty Mudstone	L-M. Bathonian			168.2	2.4
Terminilletto (IT)	Cherty Mudstone	L-M. Bathonian			169.4	2.2
Htes Alpes, Chabrières (FR)	Nodular Mudstone	U. Oxfordian	Bimammatum	Semimammatum	155.4	2.8
Htes Alpes, Chabrières (FR)	Nodular Mudstone	U. Oxfordian	Bimammatum	Semimammatum	155.5	2.9
Htes Alpes, Chabrières (FR)	Nodular Mudstone	U. Oxfordian	Bimammatum	Semimammatum	155.6	2.8
Htes Alpes, Chabrières (FR)	Nodular Mudstone	U. Oxfordian	Bimammatum	Semimammatum	155.7	2.7
Htes Alpes, Chabrières (FR)	Nodular Mudstone	U. Oxfordian	Bifurcatus	Grossouvrei	155.8	2.6
Htes Alpes, Chabrières (FR)	Nodular Mudstone	U. Oxfordian	Bifurcatus	Grossouvrei	155.8	2.9
Htes Alpes, Chabrières (FR)	Nodular Mudstone	U. Oxfordian	Bifurcatus	Grossouvrei	155.8	2.8
Htes Alpes, Chabrières (FR)	Nodular Mudstone	U. Oxfordian	Bifurcatus	Grossouvrei	155.8	2.5
Htes Alpes, Chabrières (FR)	Nodular Mudstone	U. Oxfordian	Bifurcatus	Grossouvrei	155.8	2.7
Htes Alpes, Chabrières (FR)	Nodular Mudstone	U. Oxfordian	Bifurcatus	Stenocycloides	156.0	2.9
Htes Alpes, Chabrières (FR)	Nodular Mudstone	M. Oxfordian	Transversarium	Luciaeformis	156.7	2.6
Htes Alpes, Chabrières (FR)	Nodular Mudstone	M. Oxfordian	Transversarium	Luciaeformis	156.8	2.6
Htes Alpes, Chabrières (FR)	Nodular Mudstone	M. Oxfordian	Transversarium	Luciaeformis	156.9	2.9
Htes Alpes, Chabrières (FR)	Nodular Mudstone	M. Oxfordian	Transversarium	Parandieri	157	3.1
Htes Alpes, Chabrières (FR)	Nodular Mudstone	M. Oxfordian	Transversarium	Parandieri	157.1	3
Htes Alpes, Chabrières (FR)	Nodular Mudstone	M. Oxfordian	Transversarium	Parandieri	157.2	3.1
Htes Alpes, Chabrières (FR)	Nodular Mudstone	M. Oxfordian	Plicatilis	Antecedens	157.5	3.7
Camposilvano (IT)	Nodular Mudstone	M. Oxfordian	Transversarium		156.9	3.3
Camposilvano (IT)	Nodular Mudstone	M. Oxfordian	Transversarium		157	3
Camposilvano (IT)	Nodular Mudstone	M. Oxfordian	Transversarium		157.1	3.3
Camposilvano (IT)	Nodular Mudstone	M. Oxfordian	Plicatilis		157.3	3.5
Camposilvano (IT)	Nodular Mudstone	M. Oxfordian	Plicatilis		157.4	3
Camposilvano (IT)	Nodular Mudstone	M. Oxfordian	Plicatilis		157.5	2.8
Camposilvano (IT)	Nodular Mudstone	M. Oxfordian	Plicatilis		157.6	2.9
Camposilvano (IT)	Nodular Mudstone	U. Callovian	Athleta	Spinosum	160	3
Camposilvano (IT)	Nodular Mudstone	U. Callovian	Athleta	Spinosum	160.1	3
Camposilvano (IT)	Nodular Mudstone	M. Callovian	Coronatum		161.1	3.1
Camposilvano (IT)	Nodular Mudstone	L. Callovian	Calloviense	Enodatum	162.1	2.9
Camposilvano (IT)	Nodular Mudstone	Bath/Callov.			164.4	2.6
Camposilvano (IT)	Nodular Mudstone	U. Bathonian			164.6	2.5
Camposilvano (IT)	Nodular Mudstone				165	2.8
Camposilvano (IT)	Nodular Mudstone				165.5	2.8
Camposilvano (IT)	Nodular Mudstone				166	2.7
Camposilvano (IT)	Nodular Mudstone				166.5	2.5
Camposilvano (IT)	Nodular Mudstone	M. Bathonian			166.9	2.7
Camposilvano (IT)	Nodular Mudstone	L-M. Bathonian			167.9	2.3
Camposilvano (IT)	Nodular Mudstone	L-M. Bathonian			168.9	2.7

APPENDIX E

TABLE E1

Oxygen isotope composition of apatite enamel from shark and fish teeth of the Middle and Upper Jurassic in western Europe (East France, Switzerland) (figs. 3, 4 and 5)

Taxa	Locality	Stratigraphy	Standard zonation		Marker-bed	Age	$\delta^{18}O$ $(PO_4)^1$	T °C[2]
			(ammonite zones)	(ammonite subzones)	(brachiopod)	(Ma)	‰ (SMOW)	($\delta^{18}Ow$= -1)
Pycnodont	Ste-Croix-Vaud (CH)	U. Kimmeridgian				151.5	21.4	15.0
Pycnodont	Jura, Daulencourt	U. Kimmeridgian	[Mutabilis-Eudoxus]			152.2	20.2	20.4
Asteracanthus	Saône & Loire, Flacé-les-Mâcon	L. Kimmeridgian	[Planula-Platynota]			154.0	19.7	22.4
Asteracanthus ornatissimus	Yonne, Tonnerre	U. Oxfordian	Planula			154.2	19.7	22.4
Pycnodont	Gächlingen (CH)	U. Oxfordian	Bimammatum			155.2	20.5	19.0
Pycnodont	Côte d'Or, Mailly-le-Château	U. Oxfordian	Bifurcatus			155.9	20.6	18.6
Sphenodus longidens	Jura	U. Oxfordian	Bifurcatus			155.9	20.6	18.6
Sphenodus longidens	Jura, Chatelneuf	U. Oxfordian	Bifurcatus			155.9	20.8	17.6
Lamnidae	Siblingen (CH)	M. Oxfordian	Transversarium	Luciaeformis		156.9	21.1	16.4
Sphenodus longidens	Ardèche, Rompon	M. Oxfordian	Transversarium	Parandieri		157.1	19.3	24.1
Pycnodont	Yonne, Gigny	M. Oxfordian	Plicatilis/ Transversarium			157.2	20.9	17.4
Sphenodus longidens	Ardèche, Crussol	M. Oxfordian	Plicatilis	Vertebrale/ Antecedens		157.8	21.0	16.7
Sphenodus sp.	Ardèche, La Voulte	M. Oxfordian	Plicatilis	Vertebrale/ Antecedens		157.8	20.8	17.6
Lamnidae	Üken (CH)	L. Oxfordian	Cordatum			158.3	21.5	14.6
Asteracanthus	Jura, Salins	L. Oxfordian	Cordatum			158.3	20.4	19.4
Asteracanthus	Jura, Ornans	L. Oxfordian	Mariae/ Cordatum			158.8	20.9	17.2
Asteracanthus	Arvel (CH)	Callovian/ Oxfordian	Lamberti/ Mariae			159.4	20.5	19.0
Sphenodus longidens	Ardèche, La Voulte	U. Callovian				160.0	20.6	18.6
Asteracanthus	Côte d'Or, Talant	U. Callovian	Athleta			160.2	19.5	23.1
Asteracanthus	Côte d'Or, Prusly	U. Callovian	Athleta	Phaeinum		160.5	18.9	25.7
Asteracanthus	Côte d'Or, Etrochey	M. Callovian	Coronatum	Grossouvrei	Oxoniensis	161.1	19.2	24.6
Asteracanthus tenuis	Côte d'Or, Authoison	M. Callovian	Jason			161.5	19.1	25.2
Strophodus reticulatus	Côte d'Or, Etrochey	L. Callovian	Calloviense	Enodatum	Torqui	162.2	18.8	26.3
Pycnodont	Côte d'Or, Etrochey	L. Callovian	Calloviense	Enodatum	Torqui	162.2	20.0	21.1
Strophodus	Jura, Ornans	L. Callovian	Koenigi		Kalli	163.3	19.6	22.7
Asteracanthus	Yonne, Brion (well)	L. Callovian	Herveyi	Terebratus	Divio	163.9	20.2	20.4
Asteracanthus	Côte d'Or, Colline St-Anne	L. Callovian	Herveyi	Terebratus	Divio	163.9	19.8	22
Asteracanthus	Côte d'Or, Ladoix	L. Callovian	Herveyi	Terebratus	Divio	163.9	19.0	25.4
Strophodus reticulatus	Côte d'Or, Merey	Bathonian-Callovian	Discus-Herveyi	Discus-Klepperi	[Eudesia-Divio]	164.2	19.1	25.0
Pycnodont	Côte d'Or, Les Perrières (Dijon)	U. Bathonian	Discus	Discus	Eudesia	164.6	18.8	26.3

TABLE E1
(continued)

Taxa	Locality	Stratigraphy	Standard zonation (ammonite zones)	Standard zonation (ammonite subzones)	Marker-bed (brachiopod)	Age (Ma)	$\delta^{18}O$ $(PO_4)^1$ ‰ (SMOW)	T °C[2] ($\delta^{18}Ow$= -1)
Pycnodont	Côte d'Or, Les Perrières (Dijon)	U. Bathonian	Discus	Discus	Eudesia	164.6	18.7	26.7
Asteracanthus	Côte d'Or, Les Perrières (Dijon)	U. Bathonian	Discus	Discus	Eudesia	164.6	19.1	25.0
Asteracanthus	Yonne, Jaulges (well)	U. Bathonian	Discus	Discus	Eudesia	164.6	20.7	19.9
Asteracanthus	Côte d'Or, Nuits-St-Georges	U. Bathonian	Orbis	Hannoveranus	Digo	165.3	20.2	20.1
Pycnodont	Isère, Trept	U. Bathonian	Hodsoni		Concinna	166.4	19.3	23.8
Asteracanthus	Ain, Nantua	M. Bathonian	Morisi		[Multiplicata-Concinna]	166.8	19.6	22.8
Strophodus	Côte d'Or, Vanvey	M. Bathonian	Progracilis		[Globata-Multiplicata]	167.6	19.7	22.4
Asteracanthus	Côte d'Or, Merey	L. Bathonian	Tenuiplicatus	Tenuiplicatus	Globata	167.9	18.7	26.7
Pycnodont	Var, Bandol	L. Bathonian	Zigzag	Convergens		169.1	19.7	22.4
Asteracanthus	Saône & Loire, Hurigny	U. Bajocian	Parkinsoni	Acris		170.2	20.1	20.7

(1) O-isotope analysis at Ecole normale supérieure de Lyon

(2) Temperatures of seawater calculated according to the procedure described by Longinelli and Nuti (1973) and Lécuyer and others (1993), assuming $\delta^{18}O$ seawater = −1‰ (SMOW).

All teeth analysed come from open marine environments of eastern France and northwestern Switzerland (paleolatitude of 30°–36°N).

TABLE E2

Oxygen isotope composition of belemnite rostra in the Upper Jurassic of western Russia (figs. 3, 4 and 5)

Data Source	Locality	Stratigraphy	Original zone (Ammonite)	Standard zone (Ammonite)	Age (Ma)	$\delta^{18}O$ ‰ (PDB)	T (°C)[1] ($\delta^{18}Ow$= -1)
Riboulleau and others, 1998	Dubky (RU)	U. Kimmeridgian	Aulacostephanus eudoxus	Eudoxus	151.3	-1.4	18.2
Riboulleau and others, 1998	Dubky (RU)	U. Kimmeridgian	Aulacostephanus eudoxus	Eudoxus	151.5	-1.3	17.9
Riboulleau and others, 1998	Dubky (RU)	U. Kimmeridgian	Aulacostephanus eudoxus	Eudoxus	151.7	-0.8	15.8
Riboulleau and others, 1998	Dubky (RU)	U. Kimmeridgian	Aulacostephanus eudoxus	Eudoxus	151.9	-1.4	18.3
Riboulleau and others, 1998	Mimei (RU)	L. Kimmeridgian	Rasenia cymodoce	Cymodoce	152.4	-1.1	16.9
Riboulleau and others, 1998	Makariev (RU)	L. Kimmeridgian	Rasenia cymodoce	Cymodoce	152.7	-1	16.5
Riboulleau and others, 1998	Makariev (RU)	L. Kimmeridgian	Rasenia cymodoce	Cymodoce	153	1.2	17.5
Riboulleau and others, 1998	Makariev (RU)	L. Kimmeridgian	Rasenia cymodoce	Cymodoce	153.4	1.4	18.3
Riboulleau and others, 1998	Makariev (RU)	U. Oxfordian	Pictonia baylei	Planula	154.9	1.5	18.9
Riboulleau and others, 1998	Makariev (RU)	U. Oxfordian	Amoeboceras rosenkrantzi	Bimammatum	155.2	0.06	12.1
Riboulleau and others, 1998	Makariev (RU)	U. Oxfordian	Amoeboceras regulare	Bifurcatus	155.8	-1.8	20
Riboulleau and others, 1998	Makariev (RU)	U. Oxfordian	Amoeboceras serratum	Bifurcatus	155.9	0.5	10.4
Riboulleau and others, 1998	Makariev (RU)	M. Oxfordian	Cardioceras tenuiserratum	Transversarium	157.1	-0.15	13
Riboulleau and others, 1998	Makariev (RU)	M. Oxfordian	Cardioceras densiplicatum	Plicatilis	157.4	0.6	9.9
Riboulleau and others, 1998	Makariev (RU)	M. Oxfordian	Cardioceras densiplicatum	Plicatilis	157.7	1.8	5.7
Riboulleau and others, 1998	Makariev (RU)	L./M. Oxfordian			158.1	1.6	6.4
Riboulleau and others, 1998	Makariev (RU)	L. Oxfordian	Cardioceras cordatum	Cordatum	158.3	0.4	10.9
Riboulleau and others, 1998	Makariev (RU)	L. Oxfordian	Cardioceras cordatum	Cordatum	158.5	0.8	9.1
Veizer and others, 1999	Russia	M. Oxfordian	Amoeboceras alternoides	Transversarium	156	0.36	10.9
Veizer and others, 1999	Russia	M. Oxfordian	Amoeboceras alternoides	Transversarium	156.2	-0.87	15.9
Veizer and others, 1999	Russia	M. Oxfordian	Amoeboceras alternoides	Transversarium	156.2	-1.05	16.7
Veizer and others, 1999	Russia	M. Oxfordian	Amoeboceras alternoides	Transversarium	156.2	-0.72	15.3
Veizer and others, 1999	Russia	M. Oxfordian	Amoeboceras alternoides	Transversarium	156.4	-0.40	14.0
Veizer and others, 1999	Russia	M. Oxfordian	Amoeboceras alternoides	Transversarium	156.4	-0.71	15.2
Veizer and others, 1999	Russia	M. Oxfordian	Amoeboceras alternoides	Transversarium	156.4	-1.32	17.9
Veizer and others, 1999	Russia	M. Oxfordian	Amoeboceras alternoides	Transversarium	156.4	-1.19	17.3
Veizer and others, 1999	Russia	M. Oxfordian	Amoeboceras alternoides	Transversarium	156.4	-0.69	15.2
Veizer and others, 1999	Russia	M. Oxfordian	Amoeboceras alternoides	Transversarium	156.4	-0.94	16.2
Veizer and others, 1999	Russia	M. Oxfordian	Amoeboceras alternoides	Transversarium	156.4	-0.96	16.3
Veizer and others, 1999	Russia	M. Oxfordian	Amoeboceras alternoides	Transversarium	156.4	0.31	11.1
Veizer and others, 1999	Russia	M. Oxfordian	Amoeboceras alternoides	Transversarium	156.4	-0.34	13.7
Veizer and others, 1999	Russia	M. Oxfordian	Amoeboceras alternoides	Transversarium	156.6	-0.90	16.1
Veizer and others, 1999	Russia	M. Oxfordian	Amoeboceras alternoides	Transversarium	156.6	-0.66	15.1
Veizer and others, 1999	Russia	M. Oxfordian	Amoeboceras alternoides	Transversarium	156.6	-0.81	15.7
Veizer and others, 1999	Russia	M. Oxfordian	Amoeboceras alternoides	Transversarium	156.8	0.03	12.2
Veizer and others, 1999	Russia	M. Oxfordian	Amoeboceras alternoides	Transversarium	156.8	-0.76	15.5
Veizer and others, 1999	Russia	M. Oxfordian	Amoeboceras alternoides	Transversarium	156.8	-0.29	13.5
Veizer and others, 1999	Russia	M. Oxfordian	Amoeboceras alternoides	Transversarium	156.8	-0.51	14.4
Veizer and others, 1999	Russia	M. Oxfordian	Amoeboceras alternoides	Transversarium	156.8	0.62	9.9
Veizer and others, 1999	Russia	M. Oxfordian	Amoeboceras alternoides	Transversarium	156.8	-0.88	16.0
Veizer and others, 1999	Russia	M. Oxfordian	Amoeboceras alternoides	Transversarium	156.8	-0.24	13.3
Veizer and others, 1999	Russia	M. Oxfordian	Amoeboceras alternoides	Transversarium	156.8	0.06	12.1
Veizer and others, 1999	Russia	M. Oxfordian	Amoeboceras alternoides	Transversarium	156.8	0.55	10.2
Veizer and others, 1999	Russia	M. Oxfordian	Amoeboceras alternoides	Transversarium	156.8	-0.02	12.4
Veizer and others, 1999	Russia	L. Oxford	Cardioceras cordatum	Cordatum	159	1.18	7.8
Veizer and others, 1999	Russia	Callov/Oxford	Quenstedtoceras mariae	Mariae	159.1	0.35	10.9
Veizer and others, 1999	Russia	Callov/Oxford	Q. lamberti/mariae		159.4	1.84	5.4
Veizer and others, 1999	Russia	Callov/Oxford	Q. lamberti/mariae		159.4	2.19	4.2
Veizer and others, 1999	Russia	Callov/Oxford	Q. lamberti/mariae		159.4	1.97	5.0
Veizer and others, 1999	Russia	Callov/Oxford	Quenstedtoceras lamberti	Lamberti	159.5	1.53	6.5
Veizer and others, 1999	Russia	U. Callovian	Quenstedtoceras lamberti	Lamberti	159.5	0.75	9.4
Veizer and others, 1999	Russia	U. Callovian	Quenstedtoceras lamberti	Lamberti	159.5	0.97	8.6
Veizer and others, 1999	Russia	U. Callovian	Quenstedtoceras lamberti	Lamberti	159.5	1.03	8.3
Veizer and others, 1999	Russia	U. Callovian	Quenstedtoceras lamberti	Lamberti	159.5	1.16	7.9
Veizer and others, 1999	Russia	U. Callovian	Quenstedtoceras lamberti	Lamberti	159.6	1.58	6.3
Veizer and others, 1999	Russia	U. Callovian	Quenstedtoceras lamberti	Lamberti	159.6	1.71	5.9
Veizer and others, 1999	Russia	U. Callovian	Quenstedtoceras lamberti	Lamberti	159.6	1.34	7.2
Veizer and others, 1999	Russia	U. Callovian	Quenstedtoceras lamberti	Lamberti	159.6	1.55	6.4
Veizer and others, 1999	Russia	U. Callovian	Quenstedtoceras lamberti	Lamberti	159.6	2.16	4.3
Veizer and others, 1999	Russia	U. Callovian	Quenstedtoceras lamberti	Lamberti	159.7	1.30	7.4
Veizer and others, 1999	Russia	U. Callovian	Quenstedtoceras lamberti	Lamberti	159.7	0.45	10.5
Veizer and others, 1999	Russia	Callov/Oxford	Quenstedtoceras lamberti	Lamberti	159.7	1.35	7.2
Veizer and others, 1999	Russia	U. Callovian	Quenstedtoceras lamberti	Lamberti	159.8	1.72	5.8
Veizer and others, 1999	Russia	U. Callovian	Quenstedtoceras lamberti	Lamberti	159.8	1.76	5.7
Veizer and others, 1999	Russia	U. Callovian	Quenstedtoceras lamberti	Lamberti	159.8	1.66	6.0
Veizer and others, 1999	Russia	U. Callovian	Quenstedtoceras lamberti	Lamberti	159.8	1.92	5.1
Veizer and others, 1999	Russia	U. Callovian	Peltoceras athleta	Athleta	159.9	1.14	7.9
Veizer and others, 1999	Russia	U. Callovian	Peltoceras athleta	Athleta	160.1	1.68	6.0
Veizer and others, 1999	Russia	U. Callovian	Peltoceras athleta	Athleta	160.2	1.19	7.8
Veizer and others, 1999	Russia	U. Callovian	Peltoceras athleta	Athleta	160.3	1.24	7.6
Veizer and others, 1999	Russia	U. Callovian	Peltoceras athleta	Athleta	160.3	1.31	7.3
Veizer and others, 1999	Russia	U. Callovian	Peltoceras athleta	Athleta	160.4	0.25	11.4
Veizer and others, 1999	Russia	U. Callovian	Peltoceras athleta	Athleta	160.4	0.23	11.4
Veizer and others, 1999	Russia	U. Callovian	Peltoceras athleta	Athleta	160.5	-0.13	12.9

(1) Temperatures of seawater calculated according to the equation of Epstein and others (1953), assuming $\delta^{18}O_{seawater} = -1‰$ (SMOW)

All samples come from the western Russian platform (paleolatitude of 48°N)

References

Abbink, O., Targona, J., Brinkhuis, H., and Visscher, H., 2001, Late Jurassic to earliest Cretaceous palaeoclimatic evolution of the southern North Sea: Global and Planetary Change, v. 30, p. 231–256.

Albarède, F., 1996, Introduction to Geochemical Modeling: Cambridge, Cambridge University Press, 563 p.

Al-Thour, K. A., 1997, Facies sequences of the Middle-Upper Jurassic carbonate platform (Amran Group) in the Sana'a region, Republic of Yemen: Marine and Petroleum Geology, v. 14, p. 643–660.

Ambroggi, R., 1963, Etude géologique du versant méridional du Haut Atlas occidental et de la plaine du Souss: Notes et Mémoires du Service Géologique du Royaume du Maroc, v. 157, 322 p.

Andal, D. R., Esguerra, J. S., Hashimoto, W., Reyes, B. P., and Sato, T., 1968, The Jurassic Mansalay Formation, Southern Mindoro, Philipinnes: Geology and Paleontology of South East Asia, v. IV, p. 179–197.

Anderson, T. F., Popp, B. N., Williams, A. C., Ho, L. Z., and Hudson, J. D., 1994, The stable isotopic records of fossils from the Peterborough Member, Oxford Clay Formation (Jurassic), UK: Paleoenvironmental implications: London, Journal of the Geological Society, v. 151, p. 125–138.

Angelucci, A., Barbieri, F., Maxamed, C. M., Caynab, F. C., Franco, F., Carush, M. C., and Piccoli, G., 1983, The Jurassic stratigraphic series in Gedo and Bay Regions (southwestern Somalia): Memorie di Scienze Geologiche, v. 36, p. 73–94.

Arkell, W. J., 1956, Jurassic of the World: London, Oliver and Boyd, 806 p.

Arthur, M. A., Dean, W. E., and Pratt, L. M., 1988, Geochemical and climatic effects of increased marine carbon burial at the Cenomanian/Turonian boundary: Nature, v. 335, p. 714–717.

Aurell, M., Fernandez-Lopez, S., and Meléndez, A., 1994, The Middle-Upper Jurassic oolitic ironstone level in the Iberian Range (Spain): Géobios, v. 17, p. 549–561.

Azerêdo, A. C., Ramalho, M. M., and Wright, P., 1998, The Middle-Upper Jurassic disconformity in the Lusitanian Basin, Portugal: Cuadernos de Geologia Ibérica, v. 24, p. 99–119.

Bains, S., Norris, R. D., Corfield, R. M., and Faul, C. L., 2000, Termination of global warmth at the Palaeocene/Eocene boundary through productivity feedback: Nature, v. 407, p. 171–174.

Barale, G., Iacobidze, E., Lebanidze, Z., and Philippe, M., 1991, Podocarpoxylon svanidzei (Coniferae) du Bathonien de Tkibouli en Georgie occidentale: Neues Jahrbuch für Geologie und Paläontologie, Mh. H8, p. 443–457.

Bartolini, A., Baumgartner, P. O., and Hunziker, J., 1996, Middle and Late Jurassic carbon stable-isotope stratigraphy and radiolarite sedimentation of the Umbria-Marche Basin (Central Italy): Eclogae geologicae Helvetiae, v. 89, p. 811–844.

Baumgartner, P. A., 1984, Middle Jurassic-Early Cretaceous low-latitude radiolarian zonation based on Unitary Associations and age of Tethyan radiolarites: Eclogae geologicae Helvetiae, v. 77/3, p. 729–837.

Belin, S., and Kenig, F., 1994, Petrographic analyses of organo-mineral relationships: depositional conditions of the Oxford Clay Formation (Jurassic), UK: London, Journal of the Geological Society, v. 151, p. 153–160.

Benest, M., Elmi, S., Ouardas, T., Perriaux, J., Ghali, M., and Benhamou, M., 1995, Dynamique de la mise en place d'un cône détritique d'âge callovo-oxfordien dans le sillon intra-cratonique du Nador de Tiaret sur la marge téthysienne de l'Ouest algérien: Paris, Comptes Rendus de l'Académie des Sciences, t. 321, p. 103–110.

Ben Ismail, M., Bouaziz, S., Almeras, Y., Clavel, B., Donze, P., Enay, R., Ghenmi, M., and Tintant, H., 1989, Nouvelles données biostratigraphiques sur le Callovien et les faciès "purbecko-wealdiens" (Oxfordien à Vraconien) dans la région de Tataouine (Sud-tunisien): Bulletin de la Société géologique de France, v. 5/2, p. 353–360.

Bergerat, F., Martin, P., and Dimov, D., 1998, The Moesian Platform as a key for understanding the geodynamical evolution of the Carpatho-Balkan alpine system, *in* Crasquin-Soleau, S., and Barrier, E., editors, Stratigraphy and Evolution of Peri-Tethyan platforms: Paris, Mémoire Muséum d'Histoire Naturelle, Peri-Tethys Memoir 3, v. 177, p. 127–150.

Berner, R. A., 1998, The carbon cycle and CO_2 over Phanerozoic time: the role of land plants: Philosophical Transactions of the Royal Society of London, v. 353, p. 75–82.

Berner, R. A., and Kothavala, Z., 2001, GEOCARB III: A Revised Model of Atmospheric CO_2 over Phanerozoic Time: American Journal of Science, v. 308, p. 182–204.

Besairie, H., 1972, Géologie de Madagascar (Les Terrains Sédimentaires): Annales Géologiques de Madagascar, Fasc. XXXV, 527 p.

Beydoun, Z. R., 1966, Geology of the Arabian Peninsula, Eastern Aden Protectorat: Washington, D. C., United States Government Printing Office, Geological Survey Professional Paper 560–H, 49 p.

Biddle, K. T., Uliana, M. A., Mitchum, R. M., Fitzgerald, M. G., and Wright, R. C., 1986, The stratigraphic and structural evolution of the Magallanes Basin, southern South America, *in* Allen, P. A., and Homewood, P. W., editors, Foreland basins*:* International Association of Sedimentologists Special Publication 8, p. 41–61.

Bourseau, J. P., 1977, L'Oxfordien moyen à nodules des Terres Noires de Beauvoisin (Drôme): Lyon, Nouvelles Archives du Muséum d'Histoire Naturelle, v. 15, 116 p.

Bradshaw, M., and Challinor, A. B., 1992, Australasia, *in* Westermann, G. E. G., editor, The Jurassic of Circum Pacific: Cambridge, Cambridge University Press, p. 162–180.

Broecker, W. S., 1995, The glacial world according to Wally: Palisades, New York, Eldigio Press, 312 p.

Brunn, J. H., Graciansky de, P. C., Gutnic, M., Juteau, T., Lefèvre, R., Marcoux, J., Monod, O., and Poisson, A., 1970, Structures majeures et corrélations stratigraphiques dans les Taurides occidentales: Paris, Bulletin de la Société géologique de France, t. 7, n. 3, p. 515–556.

Busson, G., 1972, Principes, méthodes et résultats d'une étude stratigraphique du Mésozoïque saharien: Mémoires du Muséum National d'Histoire Naturelle de Paris, série C, t. XXVI, 427 p.
Cariou, E., 1984, Structure, origine et paléobiogéographie des Reineckeiidae, Ammonitina du Jurassique moyen: Paris, Comptes Rendus de l'Académie des Sciences, t. 298, n. 6, p. 245–248.
Cariou, E., Contini, D., Dommergues, J. L., Enay, R., Geyssant, J. R., Mangold, C., and Thierry, J., 1985, Biogéographie des Ammonites et évolution structurale de la Téthys au cours du Jurassique: Bulletin de la Société géologique de France, t. I, n. 5, p. 679–697.
Cariou, E., Enay, R., Atrops, F., Hantzpergue, P., Marchand, D., and Rioult, M., 1997, Oxfordian, *in* Cariou, E., and Hantzpergue, P., coordonateurs, Biostratigraphie du Jurassique ouest-européen et méditerranéen: zonations parallèles et distribution des invertébrés et microfossiles: Bulletin Centre Recherche Elf Exploration Production, v. 17, p. 79–86.
Carrigan, W. J., Cole, C. A., Colling, E. L., and Jones, P. J., 1995, Geochemistry of the Upper Jurassic Tuwaiq Mountain and Hanifa Formation Petroleum Source Rocks of Eastern Saudi Arabia, *in* Katz B. J., editor, Petroleum Source Rocks: Berlin, Springer, p. 67–87.
Charcosset, P., ms, 1998, Reconstitution d'un segment de la marge ouest-téthysienne au Bathonien dans les Grands Causses et le Bas-Languedoc: Ph.D. thesis, Université Paul Sabatier, Toulouse, 320 p.
Christopher, J. E., 1964, The Middle Jurassic Shaunavon Formation: Saskatchewan Energy and Mines, Report 95, 95 p.
Chumakov, N. M., and Frakes, L. A., 1997, Mode of origin of dispersed clasts in Jurassic shales: southern part of the Yana-Kolyma fold belt, NE-Asia: Palaeogeography, Palaeoclimatology, Palaeoecology, v. 128, p. 77–85.
Cross, T. A., 1988, Controls on coal distribution in transgressive-regressive cycles, Upper Cretaceous, Western Interior, U.S.A., *in* Wilgus, C. K., Hastings, B. S., Kendall, C. G. St., Posamentier, H. W., Ross, C. A., and Van Wagoner, J. C., editors, Sea-level changes: an integrated approach: Society of Economic Paleontologists and Mineralogists Special Publication 42, p. 371–380.
Curial, A., and Dromart, G., 1998, Apport de la sismique-reflexion et des forages à l'analyse séquentielle et géométrique des corps sédimentaires et de ses encaissants: Journées scientifiques Agence Nationale de la gestion des Déchets Radioactifs, Bar-le-Duc, Atlas des Posters, p. 25–27.
Danelian, T., and Baudin, F., 1990, Découverte d'un horizon carbonaté, riche en matière organique, au sommet des radiolarites d'Epire (Grèce): Paris, Comptes Rendus Académie Sciences, 311, p. 421–428.
Da Rocha, R. B., and Tintant, H., 1974, Sur l'extension du genre Kosmoceras dans le Callovien supérieur du Portugal méridional: Bulletin de la Société géologique du Portugal, v. 19, p. 91–94.
Davis, D. W., Sewell, R. J., and Campbell, S. D. G., 1997, U-Pb dating of Mesozoic igneous rocks from Hong Kong: London, Journal of the Geological Society, v. 154, p. 1067–1076.
Delfaud, J., ms, 1969, Essais sur la géologie dynamique du domaine aquitano-pyrénéen durant le Jurassique et le Crétacé inférieur: Thèse ès Sciences Naturelles, Faculté des Sciences de l'Université de Bordeaux, Talence, t. 1, 277 p.
Dickens, G. R., 2000, Methane oxidation during the Late Palaeocene Thermal Maximum: Paris, Bulletin de la Société géologique de France, t. 171, n. 1, p. 37–49.
Dromart, G., 1989, Deposition of Upper Jurassic fine-grained limestones in the Western Subalpine Basin: Palaeogeography, Palaeoclimatology, Palaeoecology, v. 69, p. 23–43.
Dromart, G., Crumière, J. P., Elmi, S., and Espitalié, J., 1989, Géodynamique et potentialités pétrolières d'une marge de bassin: le Jurassique de la bordure ardéchoise (France Sud-Est): Paris, Comptes Rendus Académie des Sciences, t. 309, p.1495–1502.
Dromart, G., Allemand, P., Garcia, J. P., and Robin, C., 1996, Variation cyclique de la production carbonatée au Jurassique le long d'un transect Bourgogne-Ardèche, Est-France: Paris, Bulletin de la Société géologique de France, t.167, p. 423–433.
Dromart, G., Garcia, J. P., Allemand, P., Gaumet, F., and Rousselle, B., 2002, A Volume-Based Approach to Calculation of Ancient Carbonate Accumulations: Journal of Geology, v. 110, p. 95–210.
Dromart, G., Garcia, J. P., Picard, S., Atrops, F., Lécuyer, C., and Sheppard, S. M. F., 2003, Ice Age at the Middle-Late Transition?: Earth and Planetary Science Letters, v. 213, p. 205–220.
Droste, H., 1990, Depositional cycles and source rock development in an epeiric intra-platform basin: the Hanifa Formation of the Arabian Peninsula: Sedimentary Geology, v. 69, n. 3-4, p. 281–296.
Ekart, D. D., Cerling, T. E., Montanez, I. P., and Tabor, N. J., 1999, A 400 million year carbon isotope record of pedogenic carbonate: implications for paleoatmospheric carbon dioxide: American Journal of Science, v. 299, p. 805–821.
Eliuk, L. S., 1978, The Abenaki Formation, Nova Scotia Shelf, Canada: Bulletin of Canadian Petroleum Geologists, v. 25/4, p. 424–514.
——— 1981, Abenaki update: variations along a Mesozoic carbonate shelf, Nova Scotia Shelf, Canada: Canadian Society Petroleum Geologists Annual core and field sample conference, January 1981, p. 15–19.
Elmi, S., 1967, Le Lias supérieur et le Jurassique moyen de l'Ardèche: Document du Laboratoire de Géologie de la Faculté de Lyon, v. 19, 256 p.
Enay, R., Le Nindre, Y., Mangold, C., Manivit, J., and Vaslet, D., 1987, Le Jurassique d'Arabie Saoudite centrale: nouvelles données sur la lithostratigraphie, les paléoenvironnements, les faunes d'ammonites, les âges et les corrélations, *in* Enay R., coordinateur, Le Jurassique d'Arabie Saoudite Centrale :Geobios mémoire spécial 9, p. 13–65.
Epstein, S., Buchsbaum, R., Lowenstam, H. A., and Urey, H. C., 1953, Revised carbonate-water isotopic temperature scale: Geological Society of America Bulletin, v. 64, p. 1315–1326.
Espitalié, J., Deroo, G., and Marquis, F., 1985, La pyrolyse Rock-Eval et ses applications: Revue Institut Français du Pétrole, v. 40, p. 563–784.

Fantini Sestini, N., 1968, Lower Oxfordian Ammonites from Dalichai Formation: Rivista Italiana di Paleontologia e stratigraphia, v. 74, p. 403–418.
Féraud, G., Alric, V., Fornari, M., Bertrand, H., and Maller, M., 1999, $^{40}Ar/^{39}Ar$ dating of the Jurassic volcanic province of Patagonia: migrating magmatism related to Gondwana break-up and subduction: Earth and Planetary Science Letters, v. 172, p. 83–96.
Fortwengler, D., 1989, Les "Terres Noires" d'âge Callovien supérieur à Oxfordien moyen des chaînes subalpines du Sud: Paris, Comptes Rendus Académie des Sciences, v. 308, p. 531–536.
Fortwengler, D., Marchand, D., and Bonnot, A., 1997, Les coupes de Thuoux et de Savournon (SE France) et la limite Callovien - Oxfordien: Géobios, v. 30, p. 519–540.
Gaillard, C., Rio, M., Rolin, Y., and Roux, M., 1992, Fossil chemosynthetic communities related to vents or seeps in sedimentary basins; The pseudobioherms of southeastern France compared to other world examples, *in* Beauchamp, B., and von Bitter, P. H., conveners, Chemosynthesis; geological processes and products: Palaios, v. 7, p. 451–465.
Gaillardet, J., Dupré, B., Louvat, P., and Allègre, C. J., 1999a, Global silicate weathering and CO_2 consumption rates deduced from the chemistry of large rivers: Chemical Geology, v. 159, p. 3–30.
Gaillardet, J., Dupré, B., and Allègre, C. J., 1999b, Geochemistry of large river suspended sediments: Silicate weathering or recycling tracer?: Geochimica et Cosmochimica Acta, v. 63, p. 4037–4050.
Galeazzi, J. S., 1998, Structural and Stratigraphy Evolution of the Western Malvinas Basin, Argentina: American Association of Petroleum Geologists Bulletin, v. 82, p. 596–636.
Garcia, J. P., and Dromart, G., 1997, The validity of two biostratigraphic approaches in sequence stratigraphic correlations: brachiopod zones and marker beds in the Jurassic: Sedimentary Geology, v. 114, p. 55–79.
Garcia, J. P., Laurin, B., and Sambet, G., 1996, Les associations de brachiopodes du Jurassique moyen du bassin de Paris: Bulletin de la Société géologique de France, t. 167, n. 3, p. 409–421.
Gaumet, F., Garcia, J. P., Dromart, G., and Sambet, G., 1996, Contrôle stratigraphique des faciès, géométries et profils de dépôt de la plate-forme carbonatée bourguignonne au Bathonien-Callovien : Bulletin de la Société géologique de France, t. 167, n. 3, p. 435–451.
Ghosh, P., Ghosh, P., and Bhattacharya, S. K., 2001, CO_2 levels in the Late Paleozoic and Mesozoic atmosphere from soil carbonate and organic matter, Satpura basin, Central India: Palaeogeography, Palaeoclimatology, Palaeoecology, v. 170, p. 219–236.
Goldberg, M., and Friedman, G. M., 1974, Paleoenvironments and paleogeographic evolution of the Jurassic system in southern Israel: Geological Survey of Israel Bulletin, v. 61, 44 p.
Gradstein, F. M., Agterberg, F. P., Ogg, J. G., Hardenbol, J., van Veen, P., Thiery, J., and Huang, Z., 1994, A Mesozoic time scale: Journal of Geophysical Research, v. 99, p. 24,051–24,074.
Gulisano, C. A., and Gutierrez Pleimling, A. R., 1994, Field Trip Guidebook Neuquen Basin, Neuquen Province: Argentina, Fourth International Congress on Jurassic Stratigraphy and Geology.
Gygi, R., Coe, A., and Vail, P. R., 1998, Sequence stratigraphy of the Oxfordian and Kimmeridgian stages in northern Switzerland, *in* Graciansky, P. C. de, Hardenbol J., Jacquin, T., and Vail, P. R., editors, Mesozoic and Cenozoic Sequence Stratigraphy of European Basins: Society of Economic Paleontologists and Mineralogists Special Publication 60, p. 527–544.
Habib, D., and Drugg, S. W., 1983, Dinoflagellate age of Middle Jurassic – Early Cretaceous sediments in the Blake-Bahama Basin, western North, *in* Sheridan, R. E., and Gradstein, F. M., editors, Initial Reports of the Deep Sea Drilling Project, v. 76: Washington, D. C., United States Government Printing Office, p. 623–638.
Hallam, A., 1978, Eustatic cycles in the Jurassic: Palaeogeography, Palaeoclimatology, Palaeoecology, v. 23, p. 1–32.
——— 1985, A review of Mesozoic climates: London, Journal of the Geological Society, v. 142, p. 433–445.
——— 1988, A reevaluation of Jurassic eustasy in the light of new data and the revised Exxon curve, *in* Wilgus, C. K., Hastings, B. S., Kendall, C. G. St., Posamentier, H. W., Ross, C. A., and Van Wagoner, J. C., editors, Sea-level changes: an integrated approach: Society of Economic Paleontologists and Mineralogists Special publication 42, p. 261–273.
——— 2001, A review of the broad pattern of Jurassic sea-level changes and their possible causes in the light of current knowledge: Palaeogeography, Palaeoclimatology, Palaeoecology, v. 167, p. 23–37.
Hendryx, M. S., Brassell, S. C., Carroll, A., and Graham, S., 1995, Sedimentology, Organic Geochemistry, and Petroleum Potential of Jurassic Coal Measures: Tarim, Jungar, and Turpan Basins, Northwest China: American Association of Petroleum Geologists Bulletin, v. 79, p. 929–959.
Herbin, J. P., Deroo, G., and Roucaché, J., 1983, Organic geochemistry in the Mesozoic and Cenozoic formations of site 534, Blake-Bahama Basin, western North Atlantic, *in* Sheridan, R. E., and Gradstein, F. M., editors, Initial Reports of the Deep Sea Drilling Project, v. 76: Washington, D. C., United States Government Printing Office, p. 481–496.
Hesselbo, S. P., Gröcke, D. R., Jenkyns, H. C., Bjerrum, C. J., Farrimond, P., Morgans Bell, H. S., and Green, O. R., 2000, Massive dissociation of gas hydrate during a Jurassic oceanic anoxic event: Nature, v. 406, p. 392–395.
Heydari, E., and Wade, W. J., 2002, Massive recrystallization of low-Mg calcite at high temperatures in hydrocarbon source-rocks: American Association of Petroleum Geologists Bulletin, v. 6, p. 1285–1303.
Hirsch, F., 1980, Jurassic Bivalves and Gastropods from Northern Sinai and Southern Israel: Israel Journal of Earth Sciences, v. 28, p. 128–163.
Hirsch, F., Bassoulet, J. P., Cariou, E., Conway, B., Feldman, H. R., Grossowicz, L., Honigstein, A., Owen, E. F., and Rosenfeld, A., 1998, The Jurassic of the southern Levant, *in* Crasquin-Soleau, S., and Barrier, E., editors, Epicratonic basins of Peri-Tethyan platforms: Paris, Mémoire Muséum d'Histoire Naturelle, Peri-Tethys Memoir 4, v. 179, p. 213–235.

Hudson, J. D., and Martill, D. M., 1994, The Peterborough Member (Callovian, Middle Jurassic) of the Oxford Clay Formation at Peterborough, United Kingdom: London, Journal of the Geological Society, v. 151, p. 113–124.

Imlay, R. W., and Herman, G., 1984, Upper Jurassic Ammonites from the Subsurface of Texas, Louisiana, and Mississipi, *in* Ventress, W. P. S., Bebout, D. G., Perkins, B. F., and Moore, C. H., editors, The Jurassic of the Gulf Rim: Proceedings of the Third Annual Research Conference Gulf Coast Section Society of Economic Paleontologits and Mineralogists Foundation, p. 149–170.

Isaksen, G. H., Patience, R., van Graas, G., and Jenssen, A. I., 2001, Hydrocarbon system analysis in a rift basin with mixed marine and non marine source rocks: The South Viking Graben, North Sea: American Association of Petroleum Geologists Bulletin, v. 86, p. 557–591.

Jacquin, T., Dardeau, G., Durlet, C., Graciansky, P. C. de, and Hantzpergue, P., 1998, The North-Sea Cycle: An Overview of 2nd order transgressive/regressive facies cycles in western Europe, *in* Graciansky, P. C. de, Hardenbol J., Jacquin, T., and Vail, P. R., editors, Mesozoic and Cenozoic Sequence Stratigraphy of European Basins: Society of Economic Paleontologists and Mineralogists Special Publication 60, p. 445–479.

Jakovljevic, Z., Grubic, A., and Pantic, N., 1991, The Age of Mesozoic Continental Formations on the Western Margin of the Murzuq Basin: The Geology of Libya, v. 3, p. 1583–1587.

Jenkyns, H. C., 1985, The Early Toarcian and Cenomanian-Turonian anoxic events in Europe: comparisons and contrasts: Geologische Rundschau, v. 74/3, p. 505–518.

_____ 1996, Relative sea-level change and carbon isotopes: data from the Upper Jurassic (Oxfordian) of Central and Southern Europe: Terra Nova, v. 8, p. 75–85.

Jenkyns, H. C., and Clayton, C. J., 1997, Lower Jurassic epicontinental carbonates and mudstones from England and Wales: chemostratigraphic signals and the early Toarcian anoxic event: Sedimentology, v. 44, p. 687–706.

Jenkyns, H. C., Gale, A. S., and Corfield, R. M., 1994, Carbon- and oxygen-isotope stratigraphy of the English Chalk and Italian Scaglia and its palaeoclimatic significance: Geological Magazine, v. 131, p. 1–34.

Jenkyns, H. C., Jones, C. E., Gröcke, D. R., Hesselbo, S. P., and Parkinson, D. N., 2002, Chemostratigraphy of the Jurassic System: applications, limitations and implications for palaeoceanography: London, Journal of the Geological Society, v. 159, p. 351–378.

Juignet, P., and Lebert, A., 1986, Notice explicative de la feuille Mamers à 1/50 000: Orleans, Editions du Bureau Recherches Géologiques et Minières, 38 p.

Kalna, A., ms, 1994, Etude sur les ammonites du genre Taramelliceras des sous-zones Bukowskii et Costacardia (Oxfordien inférieur) du Jura Polonais: Unpublished Rapport de Stage du Magistère des Sciences de la Terre, Ecole normale supérieure de Lyon, France, 25 p.

Kaufman, A. J., Knoll, A. H., and Narbonne, G. M., 1997, Isotopes, ice ages, and terminal Proterozoic earth history: USA, Proceedings of the National Academy of Sciences, v. 94, p. 6000–6605.

Kenig, F., Hayes, J. M., Popp, B. N., and Summons, R. E., 1994, Isotopic biochemistry of the Oxford Clay Formation (Jurassic), UK: London, Journal of the Geological Society, v. 151, p. 139–152.

Kennedy, M. J., Christie-Blick, N., and Sohl, L. E., 2001, Are Proterozoic cap carbonates and isotopic excursions a record of gas hydrate destabilization following Earth's coldest intervals?: Geology, v. 29, p. 443–446.

Knenvolden, K. A., 1998, A primer on the geological occurrence of gas hydrate, in Henriet, J. P., and Mienert, J., editors, Gas hydrates: Relevance to world margin stability and climate change: Geological Society London Special Publication 137, p. 9–30.

Lancelot, Y., and Larson, R., 1990, Site 801, *in* Lancelot, Y., and Larson, R., editors, Proceedings of the Ocean Drilling Program, Scientific Results, v. 129: College Station Texas, p. 91–170.

Landais, P., and Elie, M., 1999, Utilisation de la géochimie organique pour la détermination du paléoenvironnement et de la paléothermicité dans le callovo-oxfordien du site de l'Est de la France: Actes Journées Scientifiques CNRS/ANDRA, EDP Sciences, 1999, p. 35–58.

Lécuyer, C., Grandjean, P., O'Neil, J. R., Capetta, H., and Martineau, F., 1993, Thermal excursions in the ocean at the Cretaceous-Tertiary boundary (northern Morocco)/ The $\delta^{18}O$ record of phosphatic fish debris: Palaeogeography, Palaeoclimatology, Palaeoecology, v. 105, p. 235–243.

Lécuyer, C., Picard, S., Garcia, J. P., Sheppard, S. M. F., Grandjean, P., and Dromart, G., 2003, Thermal evolution of Tethyan surface during the Middle-Late Jurassic: Evidence from δ^{18} O values of marine fish teeth: Paleoceanography, v. 18, 1076 10.1029/2002PA000863.

Legarreta, L., 1991, Evolution of a Callovian – Oxfordian carbonate margin in the Neuquen Basin of west-central Argentina: Sedimentary Geology, v. 70, p. 209–240.

Li, X., and Grant-Mackie, J. A., 1993, Jurassic sedimentary cycles and eustatic sea-levels changes in southern Tibet: Palaeogeography, Palaeaoclimatology, Palaeoecology, v. 101, p. 27–48.

Longinelli, A., and Nuti, S., 1973, Revised phosphate-water isotopic temperature scale: Earth and Planetary Science Letters, v. 19, p. 373–376.

Ludwig, W. J., and Krasheninikov, V. A., 1983, Initial Reports DSDP, 71: Washington, D. C., United States Government Printing Office, 1187 p.

Mangold, C., and Rioult, M., 1997, Bathonien, *in* Cariou, E., and Hantzpergue, P., coordonateurs, Biostratigraphie du Jurassique ouest-européen et méditerranéen: zonations parallèles et distribution des invertébrés et microfossiles: Bulletin Centre Recherche Elf Exploration Production, v. 17, p. 55–62.

Marchand, D., and Thierry, J., 1997, Enregistrement des variations morphologiques et de la composition des peuplements d'ammonites durant le cycle régressif/transgressif de 2ème ordre Bathonien inférieur-Oxfordien inférieur en Europe occidentale: Paris, Bulletin de la Société géologique de France, v. 168, p. 121–132.

Marty, B., and Tolstikhin, I. N., 1998, CO_2 fluxes from mid-ocean ridges, arcs and plumes: Chemical Geology, v. 145, p. 233–248.

McLeod, A. E., Underhill, J. R., Davies, S. J., and Dawers, N. H., 2002, The influence of fault array evolution on synrift sedimentation patterns: Controls on deposition in the Strathpey-Brent-Statfjord half graben, northern North Sea: American Association of Petroleum Association Geologists Bulletin, v. 86, p. 1061–1094.

Morton, N., 1987, Jurassic subsidence history in the Hebrides, N. W. Scotland: Marine and Petroleum Geology, v. 4, p. 226–242.

Mostafa, A. R., and Younes, M. A., 2001, Significance of organic matter in recording paleoenvironmental conditions of the Safa Formation coal sequence, Maghara Area, North Sinai, Egypt: International Journal of Coal Geology, v. 47, p. 9–21.

Norris, M., and Hallam, A., 1995, Facies variations across the Middle-Upper Jurassic boundary in Western Europe and the relationship to sea level changes: Palaeogeography, Palaeoclimatology, Palaeoecology, v. 116, p. 189–245.

Ogg, J. G., Roberston, A. H. F., and Jansa, L. F., 1983, Jurassic sedimentation history of site 534, *in* Sheridan, R. E., and Gradstein, F. M., editors, Initial Reports of the Deep Sea Drilling Project, v. 76: Washington D. C., United States Government Printing Office, p. 829–884.

Olivero, D., and Atrops, F., 1996, Les séries à Zoophycos du Bathonien/Callovien de l'Arc de Castellane (SE de la France) dans la zone de transition plate-forme-bassin: Paris, Comptes Rendus de l'Académie des Sciences, v. 323, t. IIa, p. 81–88.

Othman, R., and Ward, C., 2002, Thermal maturation pattern in the southern Bowen, northern Gunnedah and Surat Basins, northern New South Wales, Australia: International Journal of Coal Geology, v. 51, p. 145–167.

Padden, M., Weissert, H., and de Rafelis, M., 2001, Evidence for Late Jurassic release of methane from gas hydrate: Geology, v. 29, p. 223–226.

Pagani, M., Arthur, M., and Freeman, K. H., 1999, Miocene evolution of atmospheric carbon dioxide: Paleoceanography, v. 14, p. 273–292.

Parrish, J. T., 1992, Jurassic climate and oceanography of the Pacific region, *in* Westermann, G. E. G., editor, The Jurassic of Circum Pacific: Cambridge, Cambridge University Press, p. 365–379.

Paull, C., Ussler, W., and Dillon, W., 1991, Is the extent of glaciation limited by marine gas hydrates?: Geophysical Research Letters, v. 18, p. 432–434.

Petersen, H. I., Rosenberg, P., and Andsbjerg J., 1996, Organic Geochemistry in Relation to the Depositional Environments of Middle Jurassic Coal Seams, Danish Central Graben, and Implications for Hydrocarbon Generative Potential: American Association of Petroleum Geologists Bulletin, v. 80, p. 47–62.

Peybernes, B., Bouaouda, M., Alméras, Y., Ruget, C., Cugny, P., 1987, Stratigraphie du Lias et du Dogger du bassin côtier d'Essaouira (Maroc): Comptes Rendus Académie Sciences Paris, t. 305, p. 1449–1555.

Philippe, M., and Thevenard, F., 1996, Distribution and palaecology of the Mesozoic wood genus *Xenoxylon*: palaeoclimatological implication for the Jurassic of Europe: Review of Palaeobotany and Palynology, v. 91, p. 353–370.

Picard, S., Garcia, J. P., Lécuyer, C., Sheppard, S., Capetta, H., and Emig, C., 1998, $\delta^{18}O$ values of co-existing brachiopods and fish: temperature differences and estimates of paleodepths: Geology, v. 26, p. 975–978.

Pinous, O., Sahagian, D. L., Shurygin, B. N., and Nikitenko, B. L., 1999, High-resolution sequence stratigraphy analysis and sea-level interpretation of the middle and upper Jurassic strata of the Nyurolskaya depression and vicinity (southeastern West Siberia): Marine and Petroleum Geology, v.16/3, p. 245–257.

Poulton, T. P., 1984, The Jurassic of the Canadian western Interior, from 49°N latitude to Beaufort Sea, *in* Stott D. F., and Glass, D. J., editors, The Mesozoic of Middle North America: Canadian Society of Petroleum Geologists Memoir 9, p. 15–41.

Poulton, T. P., Detterman, R. L., Hall, R. L., Jones, D. L., Peterson, J. A., Smith, P., Tipper, H. W., and Westermann, G. E. G., 1992, Western Canada and United States, *in* Westermann G. E. G., editor, The Jurassic of Circum Pacific: Cambridge, Cambridge University Press, p. 29–92.

Powers, R. W., Ramirez, L. F., Redmond, C. D., and Elberg, E. L., 1966, Geology of the Arabian Peninsula, Sedimentary Geology of Saudi Arabia: Washington, D. C., United States Government Printing Office, Geological Survey Professional Paper 560-D, 47 p.

Price, G., 1999, The evidence and implications of polar ice during the Mesozoic: Earth Sciences Review, v. 48, p. 183–210.

Pucéat E., Lécuyer C., Sheppard, S. M. F., Dromart, G., Reboulet, S., and Grandjean, P., 2003, Thermal evolution of Cretaceous Tethyan surface marine waters inferred from oxygen isotope composition of fish tooth enamels: Paleoceanography, v. 18, n. 2, p. 1029–1040.

Railsbach, L. B., 1990, Influence of changing deep ocean circulation on the Phanerozoic oxygen isotopic record: Geochimica et Cosmochimica Acta, v. 54, p. 1501–1509.

Ranarison, S., ms, 1988, Le Jurassique et le Crétacé de la région d'Antsalova, bassin de Morondava (Madagascar): Diplôme de Doctorat thesis, Université Lyon 1, 182 p.

Reboulet, S., and Atrops, F., 1995, Rôle du climat sur les migrations et la composition des peuplements d'ammonites du Valanginien supérieur du bassin vocontien (S-E de la France): Lyon, Géobios, Mémoire Spécial 18, p. 357–365.

Retallack, G. J., 2001, A 300-million-year record of atmospheric carbon dioxide from fossil plant cuticles: Nature, v. 411, p. 287–290.

Riboulleau, A., Baudin, F., Daux, V., Hantzpergue, P., Renard, M., and Zakharov, V., 1998, Evolution de la paléotempérature des eaux de la plate-forme russe au cours du Jurassique supérieur: Paris, Comptes Rendus de l'Académie des Sciences, v. 326, p. 239–246.

Riccardi, A. C., 1983, The Jurassic of Argentina and Chile, *in* Moullade, M., and Nairn, A. E. M., editors, The Phanerozoic Geology of the World, The Mesozoic II: The Netherlands, Elsevier, p. 201–264.

Riebesell, U., Zondervan, I., Rost, B., Tortell, P. D., Zeebe, R. E., and Morel, F. M. M., 2000, Reduced calcification of marine plankton in response to increased atmospheric CO_2: Nature 407, p. 364–367.
Ritts, B. D., Hanson, A. D., Zinniker, D., and Moldovan, M., 1999, Lower-Middle Jurassic Nonmarine Source Rocks and Petroleum Systems of the Northern Qaidam Basin, Northwest China: American Association of Petroleum Geologists Bulletin, v. 12, p. 1980–2005.
Rocha, R. B., and Marques, B., 1979, Le Jurassique de l'Algarve (Portugal): Granada, II Coloquio de Estratigraphia y Paleogeografia del Jurasico de Espana, p. 137–141.
Ronov, A., 1994, Phanerozoic transgressions and regressions on continents: American Journal of Science, v. 294, p. 777–801.
Sagri, M., Abbate, E., Azzaroli, A., Balestrieri, M. L., Bevenuti, M., Bruni, P., Fazzuoli, M., Ficcarelli, G., Marcucci, M., Papini, M., Pavia, G., Reale, V., Rook, L., Tecle, T. M., 1998, New data on the Jurassic and Neogene to Quaternary sedimentation in the Danakil Horst, and Northern Afar Depression, Eritrea, *in* Crasquin-Soleau, S., and Barrier, E., editors, Stratigraphy and Evolution of Peri-Tethyan platforms: Paris, Peri-Tethys Memoir 3, Mémoire Muséum d'Histoire Naturelle, v. 177, p. 193–214.
Sahagian, D. L., Pinous, O., Olferiev, A., and Zakharov, V., 1996, Eustatic curve for the Middle Jurassic – Cretaceous based on Russian platform and Siberian stratigraphy: American Association of Petroleum Geologists Bulletin, v. 80/9, p. 1433–1438.
Said, R., 1962, The Geology of Egypt: The Netherlands, Elsevier Publishing Company, 377 p.
Salvador, A., Westermann, G. E. G., Oloriz, F., Gordon, M. B., and Gursky, H. J., 1992, Meso-America, *in* Westermann, G. E. G., editor, The Jurassic of Circum Pacific: Cambridge, Cambridge University Press, p. 93–121.
Sarg, F. R., 1988, Carbonate Sequence Stratigraphy, *in* Wilgus, C. K., Hastings, B. S., Kendall, C. G. St., Posamentier, H. W., Ross, C. A., and Van Wagoner, J. C., editors, Sea-level changes: an integrated approach: Society of Economic Paleontologists and Mineralogists Special Publication 42, p. 155–181.
Sarjeant, W. A .S., Volkheimer, W., and Zhang, W. P., 1992, Jurassic palynomorphs of the Circum-Pacific region, *in* Westermann, G. E. G., editor, The Jurassic of Circum Pacific: Cambridge, Cambridge University Press, p. 273–287.
Sellwood, B. W., and McKerrow, W. S., 1974, Depositional Environments in the Lower Part of the Great Oolite Group of Oxfordshire and North Gloucestershire: Proceedings of the Geologists Association, v. 85, p. 190–210.
Sey, Y. S., Repin, Y. S., Kalacheva, E. D., Okuneva, T. M., Paraketsov, K. V., and Polubotko, I. V., 1992, Eastern Russia, *in* Westermann, G. E. G., editor, The Jurassic of Circum Pacific: Cambridge, Cambridge University Press, p. 225–245.
Seyed-Emani, K., Schairer, G., and Zeiss, A., 1995, Ammoniten aus der Dalichai-Formation (Mittlere bis Oberer Jura) und der Lar-Formation (Oberer Jura) N Emamzadeh-Hashem (Zentralalborz, Nordiran): Mitteilungen der Bayerische Staatssammlung für Paläontogie und Historische Geologie, v. 35, p. 39–52.
Sharland, P. R., Archer, R., Casey D. M., Davies, R. B., Hall, S. H., Heward, A. P., Horbury, A. D., and Simmons, M. D., 2002, Arabian Plate Sequence Stratigraphy: GeoArabia Special Publication 2, 347 p.
Sheridan, R. E., and Gradstein, F. M., 1983, Initial Reports DSDP, 76: Washington, D. C., United States Government Printing Office, 947 p.
Shu, S., Jilang L., Haihong, C., Haipo, P., Hsü, K. J., and Shelton, J. W., 1989, Mesozoic and Cenozoic Sedimentary History of South China: American Association of Petroleum Geologists Bulletin, v. 73, p. 1247–1269.
Smith, A. G., Smith, D. G., and Funnell, B. M., 1994, Atlas of Mesozoic and Cenozoic Coastlines: Cambridge, Cambridge University Press, 99 p.
Sparks, R. S. J., Bursik, M. I., Carey, S. N., Gilbert, J. S., Glaze, L. S., Sigurdsson, H., and Wood, A. W., 1997, Volcanic plumes: England, John Wiley and Sons Ltd., 574 p.
Stagg, H. M., and Exon, N. F., 1981, Geology of the Scott Plateau and Rowley Terrace: Bureau Mineral Resources Bulletin of Australian Geology and Geophysics, v. 213, p. 1–55.
Sukamto, R., and Westermann, G. E. G., 1992, Indonesia and Papua New Guinea, *in* Westermann, G. E. G., editor, The Jurassic of Circum Pacific: Cambridge, Cambridge University Press, p. 181–195.
Summerhayes, C. P., and Masran, T. C., 1983, Organic facies of Cretaceous and Jurassic sediments from Deep Sea Drilling Project Site 534 in the Blake-Bahama Basin, western North, *in* Sheridan, R. E., and Gradstein, F. M., editors, Initial Reports of the Deep Sea Drilling Project, v. 76: Washington, D. C., United States Government Printing Office, v. 76, p. 469–481.
Surlyk, F., 1991, Sequence stratigraphy of the Jurassic-Lowermost Cretaceous of East Greenland: American Association of Petroleum Geologists Bulletin, v. 75, p. 1468–1488.
Tanzanian Petroleum Development Corporation, 1989, Tanzanian Petroleum Exploration Potential: Tanzanian Government Printing Office, 34 p.
Thiry, M., 2000, Paleoclimatic interpretation of clay minerals in marine deposits: an outlook from the continental origin: Earth Sciences Review, v. 49, p. 201–221.
Thierry, J., Cariou, E., Elmi, S., Mangold, C., Marchand, D., and Rioult, M., 1997, Callovian, *in* Cariou, E., and Hantzpergue, P., coordonateurs, Biostratigraphie du Jurassique ouest-européen et méditerranéen: zonations parallèles et distribution des invertébrés et microfossiles: Bulletin Centre Recherche Elf Exploration Production, v. 17, p. 63–78.
Topchishvili, M., Lominadze, T., and Tsereteli, L., 1998, Ammonite associations and biostratigraphy of the Middle Jurassic sediments of Georgia: Cuadernos de Geologia Iberica, v. 24, p. 293–309.
Underhill, J. R., and Partington, M. A., 1993, Use of genetic sequence stratigraphy in defining and determining a regional tectonic control on the "Mid-Cimmerian unconformity" – Implications for North-Sea Basin development and the global Sea-Level Chart, *in* Weimer, P., and Posamentier, H. W., editors, Siliciclastic Sequence Stratigraphy: American Association of Petroleum Geologists Memoir 3, p. 449–492.

Vakhrameev, V. A., 1981, *Classopolis* pollen indicator of Jurassic and Cretaceous climate: International Geological Review, v. 24, p. 1190–1196.
Veizer, J., Ala, D., Azmy, K., Bruckschen, P., Buhl, F., Carden, G. A. F., Diener, A., Ebneth, S., Godderis, Y., Jasper, T., Korte, C., Pawellek, F., Podlaha, O. G., and Strauss, H., 1999, $^{87}Sr/^{86}Sr$, $\delta^{18}O$ and $\delta^{13}C$ Evolution of Phanerozoic seawater: Chemical Geology, v. 161, p. 59–88.
Vincent, E., and Berger, W. H., 1985, Carbon dioxyde and polar cooling in the Miocene: The Monterey Hypothesis, *in* Sundquist, E. T., and Broecker, W. S., editors, The Carbon Cycle and Atmospheric CO2: Natural Variations Archean to Present: Geophysical Monograph Series, v. 32, p. 455–468.
Walker, J. C. G., Hays, P. B., and Kasting, J. F., 1981, A negative feedback mechanism for long-term stabilization of Earth's surface temperature: Journal of Geophysical Research, v. 86, p. 9776–9782.
Wang, Y. G., Wang, S. E., Liu, B. P., and Yü, J. S., 1992, Eastern China, *in* Westermann, G. E. G., editor, The Jurassic of Circum Pacific: Cambridge, Cambridge University Press, p. 214–224.
Weissert, H., and Lini, A., 1991, Ice age interludes during the time of Cretaceous greenhouse climate, *in* Müller D. W., and others, editors, Controversies in Modern Geology: London, Academic Press, p. 173–191.
Weissert, H., Lini, A., Fölmi, K. B., and Kuhn, O., 1998, Correlation of Early Cretaceous carbon isotope stratigraphy and platform drowning events: a possible link?: Palaeogeography, Palaeoclimatology, Palaeoecology, v. 137, p. 189–203.
Wood, R., 1999, The Evolution of Reefs and Carbonate Production, *in* Biological Participation in the Global Carbonate Cycle: Paris, La Fondation des Treilles.
Wright, J. K., 1981, The Corallian rocks of North Dorset: London, Proceedings of the Geologists Association, v. 92, p. 17–32.
——— 1986, A new look at the stratigraphy, sedimentology, and ammonite fauna of the Corallian Group (Oxfordian) of south Dorset: London, Proceedings of the Geologists Association, v. 97, p. 1–21.
Wyatt, R. J., 1996, A correlation of the Bathonian succession between Bath and Burford, and its relation to that near Oxford: Proceedings of the Geologists Association, v. 107, p. 299–322.
Yapp, C. J., and Poths, H., 1996, Carbon isotopes in continental weathering environments and variations in ancient atmospheric CO_2 pressure: Earth and Planetary Science Letters, v. 137, p. 71–82.
Zhou, Z. Y., and Lao, Q. Y., 1990, Mesozoic tectonic evolution of eastern Fujian and adjacent areas, *in* Wiley, T. J., Howell, D. G., and Wong, F. L. editors, Terrane analysis of China and the Pacific rims: Circum-Pacific Council for Energy and Mineral Resources Earth Sciences Series, v. 13, p. 285–287.
Ziegler, P. A., 1988, Evolution of the Arctic-North Atlantic and the western Tethys: American Association Petroleum Geologists Memoir 43, 198 p.